Research Article

Muserat Shaheen, Muhammad Abbas*, Farah Aini Abdullah*, and Yasser Salah Hamed

A new numerical technique for the solution of time-fractional nonlinear Klein–Gordon equation involving Atangana–Baleanu derivative using cubic B-spline functions

https://doi.org/10.1515/phys-2025-0131
received October 24, 2024; accepted January 28, 2025

Abstract: One of the earliest attempts to make special relativity and quantum mechanics compatible was the Klein–Gordon equation (KGE). In the 1920s, Oskar Klein and Walter Gordon independently proposed it. This equation plays a very significant role in the fields of quantum mechanics and quantum field theory. This equation has been solved using a variety of techniques. The current work presents a numerical approach that uses cubic B-spline (CBS) functions to solve the KGE involving Atangana–Baleanu fractional derivative. The fractional derivative in time is discretized using a finite difference scheme in the proposed technique, while the space direction is discretized using a θ-weighted scheme based on CBS functions. The Fourier approach is used to prove that the proposed scheme is unconditionally stable. A second-order convergence in the temporal and spatial directions has been proved theoretically and numerically. Finally, four applications of the KGE show the efficiency and accuracy of the proposed method than other methods.

Keywords: time-fractional nonlinear Klein–Gordon equation, finite difference scheme, cubic B-spline functions, stability, convergence, Atangana–Baleanu fractional derivative

*** Corresponding author: Muhammad Abbas,** Department of Mathematics, University of Sargodha, 40100 Sargodha, Pakistan, e-mail: muhammad.abbas@uos.edu.pk
*** Corresponding author: Farah Aini Abdullah,** School of Mathematical Sciences, Universiti Sains Malaysia, 11800 USM Pulau Pinang, Malaysia, e-mail: farahaini@usm.my
Muserat Shaheen: Department of Mathematics, University of Sargodha, 40100 Sargodha, Pakistan
Yasser Salah Hamed: Department of Mathematics and Statistics, College of Science, Taif University, P. O. Box 11099, Taif 21944, Saudi Arabia

1 Introduction

One of the most used mathematical functions for estimating processes is the spline functions. Spline functions are identified as piecewise polynomial functions that are used to solve many ordinary differential equations and partial differential equations. In recent work, these functions are also widely used to solve fractional partial differential equations. Compared to traditional differential equations, fractional order differential equations may be able to explain dynamic processes more effectively. The researchers of the twentieth century have done an astounding quantity of research on fractional calculus [1]. Caputo and Febrizio [2] presented a new definition of fractional derivative with a smooth kernel. The caputo fractional derivative is used by Diethelm and Ford [3] to solve multi-order fractional differential equations. El-Sayed *et al.* [4] investigated the fractional-order logistic equation's numerical solution, existence, stability, and uniqueness. The relativistic Klein–Gordon equation (KGE) describes spinless particles and is a version of the Schrödinger equation. Numerous mathematicians have solved the KGE using various methods, such as Shakeri and Dehghan [5] used the variational iteration method to find the analytical and approximate solution of this equation. Onate *et al.* [6] analytically derived both the energy equation and the accompanying unnormalized wave function. Gorka [7] used the Galerkin technique, the logarithmic Sobolev inequality, and the compactness theorem to find out the existence of a unique solution. Kumbinarasaiah [8] calculate a nonlinear solution of KGE by transforming a system of nonlinear algebraic equations. Lou and Chen [9] defined some unique kinds of solutions to Kleine–Gordon reduction equations. Chatterjee [10] solved the KGE iteratively using an $\frac{1}{N}$ expansion approach to get the energy spectrum of a scalar particle in a spherically symmetric potential. Subasi and Araz [11] examined the phases involved in determining the best control and the methods for approximating this control,

respectively. Atangana and Araz [12] used the recently presented numerical approach to integral and partial differential equations of both integer and noninteger order. Subasi *et al.* [13] investigated the optimality conditions in an optimal control problem governed by a hyperbolic problem. Dehghan and Shokri used collocation point and thin plate splines radial basis functions to approximate the solution in the study of Dehghan and Shokri [14]. Berat *et al.* [15] used a cubic B-spline (CBS) collocation finite element method and L_2 algorithm for the solution of the time fractional (TF) nonlinear KGE. Bratsos [16] solved the nonlinear KGE by using a predictor–corrector technique based on the application of rational approximates of second-order to the matrix-exponential term in a three-time level recurrence relation. Zhang *et al.* [17] introduced a simple direct space–time meshless approach based on the radial or nonradial basis function for the one-dimensional KGE. Shakeri and Dehghan [18] used He's variational iteration method to give approximate and analytical solutions for this equation.

Ganji *et al.* [19] presented a novel method for solving the time fractional Klein–Gordon equation (TFKGE) by employing the clique polynomial as the basis function for the operational matrices in his article. Saifullah *et al.* [20] solved the nonlinear KGE with the Caputo fractional derivative. In order to solve a set of linear and nonlinear fractional KGEs that arise in quantum and classical relativistic physics, Liu *et al.* [21] offered an analytical and numerical method. Bentrcia and Mennouni [22] discussed behavior analysis of solutions to a TFKGE in a multidimensional a bounded domain. Chen *et al.* [23] considered the numerical approximation of a nonlinear TFKGE in a bounded domain. Mohebbi *et al.* [24] investigated three equations in his article which are the TF Cattaneo equation and the linear time-fractional KG plus dissipative KG equations. They solved the TF derivative described in Caputo's sense by a scheme of order $O(\tau^{3-\alpha}), 1 < \alpha < 2$, and the space derivative is discretized with a fourth-order compact procedure. Hassani *et al.* [25] solved the variable order nonlinear TFKGE by using a set of basis functions, namely the generalized polynomials and the Caputo-type definition. As there are a number of equations with fractional derivative but this article is concerned with the following nonlinear TFKGE:

$$\begin{aligned} &\frac{\partial^\alpha U(y,s)}{\partial s^\alpha} + \mu_1 \frac{\partial^2 U(y,s)}{\partial y^2} + \mu_2 U(y,s) + \mu_3 U^\sigma(y,s) \\ &\quad = f(y,s), \\ &s \in [0,T], \quad y \in [\mathfrak{a},\mathfrak{b}], 1 < \alpha \le 2, \end{aligned} \tag{1.1}$$

with ICs:

$$U(y,0) = U_0(y), \quad U_s(y,0) = f_1(y), \quad \mathfrak{a} \le y \le \mathfrak{b}, \tag{1.2}$$

and boundary conditions (BCs)

$$U(\mathfrak{a},s) = f_2(s), \quad U(\mathfrak{b},s) = f_3(s), \quad s \ge 0, \tag{1.3}$$

where $\frac{\partial^\alpha U(y,s)}{\partial s^\alpha}$ is the Atangana–Baleanu time fractional derivative (ABTFD). Displacement of wave at point (y,s) is represented by $U(y,s)$, fractional order of the time derivative is represented by α, where $\alpha \in (1,2]$, μ_1, μ_2, and μ_3 are real numbers, $f(y,s)$ is the source term, and $\sigma = 2$ or 3.

A generalization of the KGE that takes into account fractional time derivatives and nonlinearity is the nonlinear TFKGE. Because it can realistically describe memory effects, anomalous diffusion, and complicated wave processes, this equation is important in many areas of physics, applied mathematics, and engineering. Memory effects are introduced by the fractional time derivative, which means that the system's current state is dependent on its complete past. In situations where traditional integer-order equations are ineffective, this is helpful for simulating complicated materials, viscoelasticity, and anomalous diffusion. Fractional KG models describe quantum fields having aberrant or fractal features in relativistic quantum mechanics. Nonlinear wave processes in complex and dispersive mediums are governed by the equation. Fractional derivatives make it possible to represent wave dispersion and attenuation in biological systems, optical fibers, and plasma waves more accurately. Fractional dynamics is used in inflationary cosmology to model cosmic inflation, dark energy, and early universe variations. The evolution of scalar fields in curved space–time is described by it. Kinks and domain walls are examples of soliton solutions that arise in condensed matter physics and cosmology as a result of the nonlinear KGE. It talks about localized oscillating waves called breather solutions.

Vivas-Cortez *et al.* [26] used the extended CBS functions and Caputo TF derivative for the numerical solutions of the generalized nonlinear TFKGE. Ahmad *et al.* [27] examined the Casson hybrid nanofluid's magnetohydrodynamic flow along a vertical open channel while accounting for Newtonian heating and viscous dissipation. Ahmad *et al.* [28] considered a mathematical model for the disease dynamics in both prey and predator by considering the susceptible-infected-recovered-susceptible model with the prey–predator Lotka–Volterra differential equations. Ahmad *et al.* [29] introduced a model of pine wilt disease in trees that takes into account the relationship between nematodes and transmitting beetles with pine trees that are asymptomatic and those that are symptomatic. Ain *et al.* [30] solved the nonlinear TFKGE by using a redefined extended CBS and Caputo fractional derivative. Sarboland and Aminataei [31]

applied the multi-quadratic quasi-interpolation scheme and the integrated radial basis function network scheme to solve TFKGE. Amin *et al.* [32] introduced the Haar collocation method to construct a numerical method for solving multi-term fractional differential equations up to fourth order. Amin *et al.* [33] developed the Haar collocation algorithm to solve the first-order HIV infection CD4+ T-cells model. Saeed and ur Rehman [34] suggested a technique for solving the fractional delay differential equations that make use of the Hermite wavelet approach and the method of steps. Mohammadi and Cattani [35] generalized the classical Legendre wavelet to a new fractional-order wavelet foundation. Amin *et al.* [36] created a novel collocation technique based on the Haar wavelet for the numerical solution of the fractional Volterra model for a species population expansion in a closed system. Yousif and Hamasalh [37] used a nonpolynomial spline fractional continuity method to calculate the Burgers-Fisher equation. Algehyne and Ibrahim [38] analyzed the severe acute respiratory syndrome corona virus-utilizing contemporary calculus and the Atangana–Bleanu Caputo-fractional derivative. Al-Raeei [39] simulate the spatial version of the fractional Schrödinger equation for the electrical screening potential using the Riemann–Liouville definition of fractional derivatives and numerical simulation methods. Zhang *et al.* [1] suggested a simple and direct space–time meshless approach based on the radial or nonradial basis function for the one-dimensional KGEs.

In this article, the CBS functions are used to obtain the approximate solution of TFKGE. For spatial integration, the CBS functions are used. The ABTFD is discretized by using usual a finite central difference approach. Stability and convergence are computed to demonstrate the scheme's effectiveness. To demonstrate the correctness of the proposed approach, four test examples are provided along with comparisons to existing problems in the literature. Some results in the form of tables and graphs are provided for verification and correctness of the proposed scheme.

This article is organized as follows. Section 2 has several significant definitions. Section 3 provides an explanation of the method's description, where Section 4 contains the initial vector. Stability and convergence are found in Sections 5 and 6, respectively. The numerical examples and closing remarks are given in Sections 7 and 8, respectively.

2 Preliminaries

Definition 1. Suppose that $s > \mathfrak{a}$, $\alpha > 0$, and $\alpha, \mathfrak{a}, s \in \mathbb{R}$, then the ABTFD of order α of a function $U(y, s) \in H^n(\mathfrak{a}, \mathfrak{b})$, $\mathfrak{b} > \mathfrak{a}$ was shown by Atangana and Baleanu [40] to be

$$
{}^{AB}_{\mathfrak{a}}D_s^{\alpha}U(y,s) = \begin{cases} \dfrac{A_B(\alpha)}{(n-\alpha)}\displaystyle\int_{\mathfrak{a}}^{s}\frac{d^n}{\mathrm{d}\tau^n}U(y,\tau)E_{\alpha}\Big[& n-1<\alpha<n\in\mathbb{N}, \\ \quad -\dfrac{\alpha}{n-\alpha}(s-\tau)^{\alpha}\Big]\mathrm{d}\tau, & \\ \dfrac{d^n}{\mathrm{d}s^n}U(y,s), & \alpha=n\in\mathbb{N}, \end{cases}
$$

where $A_B(\alpha)$ is a function that has been normalized and has the characteristic $A_B(\alpha = n - 1) = 1 = A_B(\alpha = n)$. $E_{\alpha,\tau}(s)$ is the Mittag–Leffler function (MLF) of two parameters with $E_{\alpha,1}(s) = E_{\alpha}(s)$, defined as [41]

$$
E_{\alpha,\tau}(s) = \sum_{\nu=0}^{\infty}\frac{s^{\nu}}{\Gamma(\alpha\nu+\tau)}.
$$

The MLF has many properties, some of them are given by Shukla and Prajapati [42].

The ABTFD is a modern concept in fractional calculus, which provides advantages in modeling complex systems with memory and hereditary properties. Some of its advantages include generalization of classical models, inclusion of non-singular kernels, better representation of memory effects, physical interpretability, flexibility in applications, and preservation of initial conditions (ICs). ABTFD is based on the generalized Mittag–Leffler kernel, which gives it a nonlocal and memory-preserving nature, while the conformable derivative is a straightforward extension of the classical derivative, designed to maintain some of the intuitive properties of derivatives for fractional orders. With memory effects, the Atangana–Baleanu fractional derivative offers a strong framework for simulating complex structures. However, for broader applicability, its few shortcomings in terms of BC formulation and limited analytical solutions must be addressed.

Definition 2. If $w \in L^2[\mathfrak{a}, \mathfrak{b}]$, then Parseval's identity is given as [43]

$$
\sum_{m=-\infty}^{\infty}|\hat{w}(p)|^2 = \int_{\mathfrak{a}}^{\mathfrak{b}}|w(q)|^2\mathrm{d}r, \tag{2.1}
$$

where $\hat{w}(p) = \int_{\mathfrak{a}}^{\mathfrak{b}}w(q)e^{2\pi ipq}\mathrm{d}r$ is the Fourier transform for every integer p.

2.1 CBS functions

The CBS functions offer several advantages over other collocation methods, particularly in solving differential equations and related mathematical modeling problems. The CBS functions are smooth, C^2 continuous, stable, and they

provide more accurate numerical results due to their numerous geometrical aspects, such as symmetrical characteristics, convex hull features, locally supportive qualities, nonnegativity, and a partition of unity [43]. The CBS collocation method provides the numerical results in the form of a cubic piecewise function. It also has a speciality to calculate the solutions at each grid point than other finite difference schemes.

The interval $[\mathfrak{a}, \mathfrak{b}]$ is partitioned into $\mathcal{N}$ subintervals represents the spatial domain. In this interval $\mathfrak{a} = y_0 < y_1 < y_2 < y_3 < \ldots < y_{\mathcal{N}-1} < y_{\mathcal{N}} = \mathfrak{b}$, where $y_i = y_0 + ih$, $i = 0(1)\mathcal{N}$ and spatial length $h = \frac{\mathfrak{b}-\mathfrak{a}}{\mathcal{N}}$. Let us consider that $u(y, s)$ is the CBS approximation for $U(y, s)$ s.t.

$$u(y, s) = \sum_{i=-1}^{\mathcal{N}+1} \psi_i^k(s) G_i(y). \tag{2.2}$$

Here, $\psi_i^k(s)$ are unknown time-dependent control points that are needed to compute at each time knot and $G_i(y)$ are the CBS functions. These CBS functions can be defined as [44]

$$G_i(y) = \frac{1}{6h^3}\begin{cases} (y - y_{i-2})^3, & y \in [y_{i-2}, y_{i-1}), \\ h^3 + 3h^2(y - y_{i-1}) + 3h(y - y_{i-1})^2 & y \in [y_{i-1}, y_i), \\ \quad - 3(y - y_{i-1})^3, & \\ h^3 + 3h^2(y_{i+1} - y) + 3h(y_{i+1} - y)^2 & y \in [y_i, y_{i+1}), \\ \quad - 3(y_{i+1} - y)^3, & \\ (y_{i+2} - y)^3, & y \in [y_{i+1}, y_{i+2}), \\ 0, & \text{Otherwise}. \end{cases} \tag{2.3}$$

At nodal points, the values of u, u_y, and u_{yy} can be found in terms of unknown parameter $\psi_i^k(s)$. Moreover, the basis splines of third degree $G_{-1}, G_0, G_1, \ldots, G_{\mathcal{N}}$ have been organized. Eqs. (2.2) and (2.3) give the following approximations:

$$\begin{cases} (u)_i^k = \frac{1}{6}\psi_{i-1}^k + \frac{4}{6}\psi_i^k + \frac{1}{6}\psi_{i+1}^k, \\ (u_y)_i^k = \frac{1}{2h}\psi_{i+1}^k - \frac{1}{2h}\psi_{i-1}^k, \\ (u_{yy})_i^k = \frac{1}{h^2}\psi_{i-1}^k - \frac{2}{h^2}\psi_i^k + \frac{1}{h^2}\psi_{i+1}^k. \end{cases} \tag{2.4}$$

3 Description of the numerical method

The ABTFD has been utilized to discretize the TF term of presented problem. Assume that K equal subintervals of length $\Delta s = \frac{S}{K}$ split the time domain $[0, S]$, using the knots $0 = s_0, s_1, \ldots, s_K = S$, where $s_k = k\Delta s$, $k = 0, 1, \ldots, K$. Now, ABTFD can be discretized as

$$\begin{aligned} &\frac{\partial^\alpha}{\partial s^\alpha} U(y, s_{k+1}) \\ &= \frac{AB(\alpha)}{2-\alpha} \int_0^{s_{k+1}} \frac{\partial^2}{\partial v^2} U(y, v) E_\alpha\left[-\frac{\alpha}{2-\alpha}(s_{k+1} - v)^\alpha\right] \mathrm{d}v, \\ &\quad 1 < \alpha < 2, \\ &= \frac{AB(\alpha)}{2-\alpha} \sum_{l=0}^{k} \int_{s_l}^{s_{l+1}} \frac{\partial^2}{\partial v^2} U(y, v) E_\alpha\left[-\frac{\alpha}{2-\alpha}(s_{k+1} - v)^\alpha\right] \mathrm{d}v. \end{aligned} \tag{3.1}$$

Theoretically robust and easy to implement, finite difference schemes are a popular tool in scientific computing, particularly for problems with regular domains and simple BCs. Through forward finite difference formulation, Eq. (3.1) is modified as

$$\begin{aligned} &\frac{\partial^\alpha}{\partial s^\alpha} U(y, s_{k+1}) \\ &= \frac{AB(\alpha)}{2-\alpha} \sum_{l=0}^{k} \frac{U(y, s_{l+1}) - 2U(y, s_l) + U(y, s_{l-1})}{(\Delta s)^2} \\ &\quad \times \int_{s_l}^{s_{l+1}} E_\alpha\left[-\frac{\alpha}{2-\alpha}(s_{k+1} - v)^\alpha\right] \mathrm{d}v + \hbar_{\Delta s}^{k+1}, \\ &= \frac{AB(\alpha)}{\Delta s(2-\alpha)} \sum_{l=0}^{k} [U(y, s_{k-l+1}) - 2U(y, s_{k-l}) + U(y, s_{k-l-1})] \\ &\quad \times (l+1) E_{\alpha,2}[-\frac{\alpha}{2-\alpha}((l+1)\Delta s)^\alpha] \\ &\quad - l E_{\alpha,2}[-\frac{\alpha}{2-\alpha}(l\Delta s)^\alpha] + \hbar_{\Delta s}^{k+1}, \\ &= \frac{AB(\alpha)}{\Delta s(2-\alpha)} \sum_{l=0}^{k} [U(y, s_{k-l+1}) - 2U(y, s_{k-l}) + U(y, s_{k-l-1})] \\ &\quad \times ((l+1)\tilde{E}_{l+1} - l\tilde{E}_l) + \hbar_{\Delta s}^{k+1}. \end{aligned}$$

Hence

$$\begin{aligned} \frac{\partial^\alpha}{\partial s^\alpha} U(y, s_{k+1}) = \frac{AB(\alpha)}{\Delta s(2-\alpha)} \sum_{l=0}^{k} q_l [U(y, s_{k-l+1}) \\ - 2U(y, s_{k-l}) + U(y, s_{k-l-1})] + \hbar_{\Delta s}^{k+1}, \end{aligned} \tag{3.2}$$

where $\tilde{E}_l = E_{\alpha,2}[-\frac{\alpha}{2-\alpha}(l\Delta s)^\alpha]$ and $q_l = ((l+1)\tilde{E}_{l+1} - l\tilde{E}_l)$. Furthermore, the truncation error $\hbar_{\Delta s}^{k+1}$ is indicated as

$$|\hbar_{\Delta s}^{k+1}| \le \Upsilon(\Delta s)^2, \tag{3.3}$$

where Υ is a constant.

Using the θ-weighted scheme and Eqs. (3.2) and (1.1) takes the form

$$\begin{aligned} &\frac{AB(\alpha)}{\Delta s(2-\alpha)} \sum_{l=0}^{k} q_l [U(y, s_{k-l+1}) - 2U(y, s_{k-l}) \\ &\quad + U(y, s_{k-l-1})] + \theta(\mu_1 U_{yy}(y, s_{k+1}) + \mu_2 U(y, s_{k+1})) \\ &\quad + (1-\theta)(\mu_1 U_{yy}(y, s_k) + \mu_2 U(y, s_k)) \\ &\quad = -\mu_3 (U(y, s_k))^\sigma + f(y, s_{k+1}). \end{aligned} \tag{3.4}$$

A numerical technique for solving differential equations that offer a modifiable trade-off between explicit, Crank–Nicolson, and implicit time-stepping is the θ-weighted scheme. The method is totally implicit when $\theta = 1$, fully explicit when $\theta = 0$, and the Crank–Nicolson approach when $\theta = 0.5$. We adopt $\theta = 1$ for the direction of space throughout the work, Eq. (3.4) yields

$$\beta\sum_{l=0}^{k} q_l[U_\iota^{k-l+1} - 2U_\iota^{k-l} + U_\iota^{k-l-1}] + \mu_1(U_{yy})_\iota^{k+1} + \mu_2 U_\iota^{k+1} = -\mu_3(U^\sigma)_\iota^k + f_\iota^{k+1}, \qquad k = 0, 1, \ldots, K, \tag{3.5}$$

where $\beta = \frac{AB(\alpha)}{\Delta s(2-\alpha)}$, $U_\iota^k = U(y_\iota, s_k)$, and $f_\iota^{k+1} = f(y_\iota, s_{k+1})$. After rearrangement, Eq. (3.5) yields

$$\begin{aligned}(\beta E_1 + \mu_2)U_\iota^{k+1} + \mu_1(U_{yy})_\iota^{k+1} &= 2\beta E_1 U_\iota^k - \beta E_1 U_\iota^{k-1} - \beta\sum_{l=1}^{k} q_l[U_\iota^{k-l+1} - 2U_\iota^{k-l} \\ &\quad + U_\iota^{k-l-1}] - \mu_3(U^\sigma)_\iota^k + f_\iota^{k+1}.\end{aligned} \tag{3.6}$$

It is clear that when $l = k$ or $k = 0$, the term U^{-1} is obtained. To handle this term, the ICs is used by the help of central difference approximation to obtain

$$U^{-1} = U^1 - 2\Delta s f_1(y).$$

Using the CBS approximations and their derivatives at the particular knot y_ι in Eq. (3.6), then

$$\begin{aligned}(\beta E_1 + \mu_2)u_\iota^{k+1} + \mu_1(u_{yy})_\iota^{k+1} &= 2\beta E_1 u_\iota^k - \beta E_1 u_\iota^{k-1} - \beta\sum_{l=1}^{k} q_l[u_\iota^{k-l+1} - 2u_\iota^{k-l} + u_\iota^{k-l-1}] \\ &\quad - \mu_3(u^\sigma)_\iota^k + f_\iota^{k+1}.\end{aligned} \tag{3.7}$$

Using (2.4) in (3.7), we obtain

$$\begin{aligned}&\left[\frac{1}{6}(\beta E_1 + \mu_2) + \frac{\mu_1}{h^2}\right]\psi_{\iota-1}^{k+1} + \left[\frac{4}{6}(\beta E_1 + \mu_2) - \frac{2\mu_1}{h^2}\right]\psi_\iota^{k+1} \\ &\quad + \left[\frac{1}{6}(\beta E_1 + \mu_2) + \frac{\mu_1}{h^2}\right]\psi_{\iota+1}^{k+1} \\ &= 2\beta E_1\left(\frac{1}{6}\psi_{\iota-1}^k + \frac{4}{6}\psi_\iota^k + \frac{1}{6}\psi_{\iota+1}^k\right) - \beta E_1\left(\frac{1}{6}\psi_{\iota-1}^{k-1} + \frac{4}{6}\psi_\iota^{k-1} + \frac{1}{6}\psi_{\iota+1}^{k-1}\right) \\ &\quad - \beta\sum_{l=1}^{k} q_l\left[\frac{1}{6}(\psi_{\iota-1}^{k-l+1} - 2\psi_{\iota-1}^{k-l} + \psi_{\iota-1}^{k-l-1}) + \frac{4}{6}(\psi_\iota^{k-l+1} - 2\psi_\iota^{k-l} + \psi_\iota^{k-l-1}) \right. \\ &\quad \left. + \frac{1}{6}(\psi_{\iota+1}^{k-l+1} - 2\psi_{\iota+1}^{k-l} + \psi_{\iota+1}^{k-l-1})\right] - \mu_3\frac{T_1}{6^\sigma} + f_\iota^{k+1},\end{aligned} \tag{3.8}$$

where $T_1 = (\psi_{\iota-1}^k + 4\psi_\iota^k + \psi_{\iota+1}^k)^\sigma$. Eq. (3.8) can be written as

$$d_1\psi_{\iota-1}^{k+1} + d_2\psi_\iota^{k+1} + d_1\psi_{\iota+1}^{k+1} = Z_\iota^k, \tag{3.9}$$

where

$$\begin{aligned}d_1 &= \left[\frac{1}{6}(\beta E_1 + \mu_2) + \frac{\mu_1}{h^2}\right], \\ d_2 &= \left[\frac{4}{6}(\beta E_1 + \mu_2) - \frac{2\mu_1}{h^2}\right], \\ Z_\iota^k &= 2\beta E_1\left(\frac{1}{6}\psi_{\iota-1}^k + \frac{4}{6}\psi_\iota^k + \frac{1}{6}\psi_{\iota+1}^k\right) - \beta E_1\left(\frac{1}{6}\psi_{\iota-1}^{k-1} + \frac{4}{6}\psi_\iota^{k-1} + \frac{1}{6}\psi_{\iota+1}^{k-1}\right) \\ &\quad - \beta\sum_{l=1}^{k} q_l\left[\frac{1}{6}(\psi_{\iota-1}^{k-l+1} - 2\psi_{\iota-1}^{k-l} + \psi_{\iota-1}^{k-l-1}) + \frac{4}{6}(\psi_\iota^{k-l+1} - 2\psi_\iota^{k-l} + \psi_\iota^{k-l-1}) \right. \\ &\quad \left. + \frac{1}{6}(\psi_{\iota+1}^{k-l+1} - 2\psi_{\iota+1}^{k-l} + \psi_{\iota+1}^{k-l-1})\right] - \mu_3\frac{T_1}{6^\sigma} + f_\iota^{k+1}.\end{aligned}$$

There are $\mathcal{N} + 1$ linear equations in $\mathcal{N} + 3$ unknowns in system (3.9). In order to obtain a numerical solution of the system, the remaining two equations are extracted from the BCs, Eq. (1.3) yields

$$\begin{aligned}\frac{1}{6}\psi_1^{k+1} + \frac{4}{6}\psi_0^{k+1} + \frac{1}{6}\psi_{-1}^{k+1} &= f_2^{k+1}, \\ \frac{1}{6}\psi_{\mathcal{N}+1}^{k+1} + \frac{4}{6}\psi_{\mathcal{N}}^{k+1} + \frac{1}{6}\psi_{\mathcal{N}-1}^{k+1} &= f_3^{k+1}.\end{aligned}$$

After using BCs, an $(N + 3) \times (N + 3)$ matrix system is obtained that can be uniquely solved using any suitable numerical technique. The above-mentioned system of linear equations given in Eq. (3.9) can be written in matrix form as

$$BC^{k+1} = QC^k,$$

where

$$C^{k+1} = (\psi_{-1}^{k+1}, \psi_0^{k+1}, \psi_1^{k+1}, \ldots, \psi_{\mathcal{N}-1}^{k+1}, \psi_{\mathcal{N}}^{k+1}, \psi_{\mathcal{N}+1}^{k+1})^T,$$

$$B = \begin{pmatrix} \frac{1}{6} & \frac{4}{6} & \frac{1}{6} & 0 & \ldots & 0 & 0 & 0 & 0 \\ d_1 & d_2 & d_1 & 0 & \ldots & 0 & 0 & 0 & 0 \\ 0 & d_1 & d_2 & d_1 & \ldots & 0 & 0 & 0 & 0 \\ \vdots & \vdots & \vdots & \vdots & \ddots & \vdots & \vdots & \vdots & \\ 0 & 0 & 0 & 0 & \ldots & d_1 & d_2 & d_1 & 0 \\ 0 & 0 & 0 & 0 & \ldots & 0 & d_1 & d_2 & d_1 \\ 0 & 0 & 0 & 0 & \ldots & 0 & \frac{1}{6} & \frac{4}{6} & \frac{1}{6} \end{pmatrix}, Q = \begin{pmatrix} f_2^{k+1} \\ Z_0^{k+1} \\ Z_1^{k+1} \\ \vdots \\ Z_{\mathcal{N}-1}^{k+1} \\ Z_{\mathcal{N}}^{k+1} \\ f_3^{k+1} \end{pmatrix}.$$

4 Initial vector

The initial vector $\psi^0 = [\psi_{-1}^0, \psi_0^0, \psi_1^0, \cdot, \ldots, \psi_{\mathcal{N}+1}^0]$ is achieved by utilizing the ICs as

$$\begin{cases} (u_y)_i^0 = U_0'(y_i), & i = 0, \\ (u)_i^0 = U_0(y_i), & i = 0, 1, \ldots, \mathcal{N}, \\ (u_y)_i^0 = U_0'(y_i), & i = \mathcal{N}. \end{cases} \tag{4.1}$$

System (4.1) having $(\mathcal{N}+3)\times(\mathcal{N}+3)$ equations and unknown, respectively. It can be written in matrix form as

$$\grave{G}C^0 = P,$$

where

$$\grave{G} = \begin{pmatrix} \frac{-1}{2h} & 0 & \frac{1}{2h} & 0 & \ldots & 0 & 0 & 0 & 0 \\ \frac{1}{6} & \frac{4}{6} & \frac{1}{6} & 0 & \ldots & 0 & 0 & 0 & 0 \\ 0 & \frac{1}{6} & \frac{4}{6} & \frac{1}{6} & \ldots & 0 & 0 & 0 & 0 \\ \vdots & \vdots & \vdots & \vdots & \ddots & \vdots & \vdots & \vdots & \\ 0 & 0 & 0 & 0 & \ldots & \frac{1}{6} & \frac{4}{6} & \frac{1}{6} & 0 \\ 0 & 0 & 0 & 0 & \ldots & 0 & \frac{1}{6} & \frac{4}{6} & \frac{1}{6} \\ 0 & 0 & 0 & 0 & \ldots & 0 & \frac{-1}{2h} & 0 & \frac{1}{2h} \end{pmatrix}, C^0 = \begin{pmatrix} \psi_{-1}^0 \\ \psi_0^0 \\ \psi_1^0 \\ \vdots \\ \psi_{\mathcal{N}-1}^0 \\ \psi_{\mathcal{N}}^0 \\ \psi_{\mathcal{N}+1}^0 \end{pmatrix},$$

$$P = \begin{pmatrix} U_0'(y_0) \\ U_0(y_0) \\ U_0(y_1) \\ \vdots \\ U_0(y_{\mathcal{N}-1}) \\ U_0(y_{\mathcal{N}}) \\ U_0'(y_{\mathcal{N}+1}) \end{pmatrix}.$$

5 Stability analysis

The stability of the suggested scheme is examined in this section using the von Neumann stability method. The increase of error in a single Fourier mode is taken into account in the von Neumann analysis of stability [45]. It is well known that the stability of linear schemes can be examined using this method. It is assumed that every nonlinear term in Eq. (1.1) is zero [45]. For the sake of simplicity, we will discuss the suggested scheme's stability for the linear form of Eq. (1.1) as

$$\frac{\partial^\alpha U(y,s)}{\partial s^\alpha} + \mu_1 \frac{\partial^2 U(y,s)}{\partial y^2} + \mu_2 U(y,s) = f(y,s),$$
$$s \in [0,T], y \in [\mathfrak{a}, \mathfrak{b}], 1 < \alpha \le 2.$$

Use the technique described in Section 3 for $\theta = 1$, we have

$$\begin{aligned} &\left[\frac{1}{6}(\beta E_1 + \mu_2) + \frac{\mu_1}{h^2}\right]\psi_{i-1}^{k+1} \\ &\quad + \left[\frac{4}{6}(\beta E_1 + \mu_2) - \frac{2\mu_1}{h^2}\right]\psi_i^{k+1} \\ &\quad + \left[\frac{1}{6}(\beta E_1 + \mu_2) + \frac{\mu_1}{h^2}\right]\psi_{i+1}^{k+1} \\ &= 2\beta E_1\left(\frac{1}{6}\psi_{i-1}^k + \frac{4}{6}\psi_i^k + \frac{1}{6}\psi_{i+1}^k\right) \\ &\quad - \beta E_1\left(\frac{1}{6}\psi_{i-1}^{k-1} + \frac{4}{6}\psi_i^{k-1} + \frac{1}{6}\psi_{i+1}^{k-1}\right) \\ &\quad - \beta\sum_{l=1}^{k} q_l\left[\frac{1}{6}(\psi_{i-1}^{k-l+1} - 2\psi_{i-1}^{k-l} + \psi_{i-1}^{k-l-1})\right. \\ &\quad + \frac{4}{6}(\psi_i^{k-l+1} - 2\psi_i^{k-l} + \psi_i^{k-l-1}) \\ &\quad \left. + \frac{1}{6}(\psi_{i+1}^{k-l+1} - 2\psi_{i+1}^{k-l} + \psi_{i+1}^{k-l-1})\right]. \end{aligned} \tag{5.1}$$

Let us use the Fourier approach now [46,47] and assume that the growth factor is represented by the symbol $\varnothing_i^k$. Its estimation can be shown as $\tilde{\varnothing}_i^k$. The error ϱ_i^k can be given as

$$\varrho_i^k = \varnothing_i^k - \tilde{\varnothing}_i^k, \; i = 1, 2, \ldots, \mathcal{N}-1, \; k = 0, 1, \ldots, K.$$

From Eq. (5.1), we obtain

$$\begin{aligned} &\left[\frac{1}{6}(\beta E_1 + \mu_2) + \frac{\mu_1}{h^2}\right]\varrho_{i-1}^{k+1} \\ &\quad + \left[\frac{4}{6}(\beta E_1 + \mu_2) - \frac{2\mu_1}{h^2}\right]\varrho_i^{k+1} \\ &\quad + \left[\frac{1}{6}(\beta E_1 + \mu_2) + \frac{\mu_1}{h^2}\right]\varrho_{i+1}^{k+1} \\ &= 2\beta E_1\left(\frac{1}{6}\varrho_{i-1}^k + \frac{4}{6}\varrho_i^k + \frac{1}{6}\varrho_{e+1}^k\right) \\ &\quad - \beta E_1\left(\frac{1}{6}\varrho_{i-1}^{k-1} + \frac{4}{6}\varrho_i^{k-1} + \frac{1}{6}\varrho_{i+1}^{k-1}\right) \\ &\quad - \beta\sum_{l=1}^{k} q_l\left[\frac{1}{6}(\varrho_{i-1}^{k-l+1} - 2\varrho_{i-1}^{k-l} + \varrho_{i-1}^{k-l-1})\right. \\ &\quad + \frac{4}{6}(\varrho_i^{k-l+1} - 2\varrho_i^{k-l} + \varrho_i^{k-l-1}) \\ &\quad \left. + \frac{1}{6}(\varrho_{i+1}^{k-l+1} - 2\varrho_{i+1}^{k-l} + \varrho_{i+1}^{k-l-1})\right]. \end{aligned} \tag{5.2}$$

From initial and BCs, it can be written as

$$\begin{aligned} &\varrho_i^0 = U_0(y), \quad \varrho_0^k = f_2(s_k), \\ &\varrho_{\mathcal{N}}^k = f_3(s_k), \quad i = 1, 2, \ldots, \mathcal{N}-1, \quad k = 0, 1, \ldots, K. \end{aligned} \tag{5.3}$$

The mesh function is described as

$$\varrho^k = \begin{cases} \varrho_i^k, & y_i - \frac{h}{2} < y \le y_i + \frac{h}{2}, i = 1, 2, \ldots, \mathcal{N}-1, \\ 0, & \mathfrak{a} \le y \le \mathfrak{a} + \frac{h}{2} \quad \text{or} \quad \mathfrak{b} - \frac{h}{2} \le y \le \mathfrak{b}. \end{cases}$$

In terms of Fourier series, $\varrho^k(y)$ can be written as

$$\varrho^k(y) = \sum_{\hat{r}=-\infty}^{\infty} \Omega^k(\hat{r}) e^{\frac{2\pi j\hat{r}y}{\mathfrak{b}-\mathfrak{a}}},$$

where

$$\Omega^k(\hat{r}) = \frac{1}{\mathfrak{b}-\mathfrak{a}}\int_{\mathfrak{a}}^{\mathfrak{b}} \varrho^k(y) e^{\frac{-2\pi j\hat{r}y}{\mathfrak{b}-\mathfrak{a}}} dy,\ k = 0, 1, \ldots, K \quad \text{and} \quad \varrho^k = [\varrho_1^k, \varrho_2^k, \ldots \varrho_{\mathcal{N}-1}^k]^T.$$

By applying norm, we obtain

$$\begin{aligned} \|\varrho^k\|_2 &= \sqrt{h \sum_{\ell=1}^{\mathcal{N}-1} |\varrho_\ell^k|^2}, \\ &= \left(\int_{\mathfrak{a}}^{\mathfrak{a}+\frac{h}{2}} |\varrho^k|^2 dy + \sum_{\ell=1}^{\mathcal{N}-1} \int_{y_\ell-\frac{h}{2}}^{y_\ell+\frac{h}{2}} |\varrho^k|^2 dy + \int_{\mathfrak{b}-\frac{h}{2}}^{\mathfrak{b}} |\varrho^k|^2 dy \right)^{\frac{1}{2}}, \\ &= \left(\int_{\mathfrak{a}}^{\mathfrak{b}} |\varrho^k|^2 dy \right)^{\frac{1}{2}}. \end{aligned}$$

By Parseval's identity (2.1), we obtain

$$\int_{\mathfrak{a}}^{\mathfrak{b}} |\varrho^k|^2 dy = \sum_{r=-\infty}^{\infty} |\Omega^k(r)|^2.$$

Hence, we achieve

$$\|\varrho^k\|_2^2 = \sum_{r=-\infty}^{\infty} |\Omega^k(r)|^2. \tag{5.4}$$

Let Eq. (5.2)–(5.3) possess a solution in the form of Fourier expansion as

$$\varrho_\ell^k = \Omega^k e^{j\varepsilon\ell h}, \tag{5.5}$$

where ε is the mode number, $j = \sqrt{-1}$. Using Eq. (5.5) in Eq. (5.3) and we obtain

$$\begin{aligned} &\Omega^{k+1}\left[\frac{1}{6}(\beta E_1 + \mu_2) + \frac{\mu_1}{h^2}\right] e^{-j\varepsilon h} \\ &\quad + \Omega^{k+1}\left[\frac{4}{6}(\beta E_1 + \mu_2) - \frac{2\mu_1}{h^2}\right] \\ &\quad + \Omega^{k+1}\left[\frac{1}{6}(\beta E_1 + \mu_2) + \frac{\mu_1}{h^2}\right] e^{-j\varepsilon h} \\ &= 2\beta E_1\left(\frac{1}{6}\Omega^k e^{j\varepsilon h} + \frac{4}{6}\Omega^k + \frac{1}{6}\Omega^k e^{-j\varepsilon h}\right) \\ &\quad - \beta E_1\left(\frac{1}{6}\Omega^k e^{j\varepsilon h} + \frac{4}{6}\Omega^k + \frac{1}{6}\Omega^k e^{-j\varepsilon h}\right) \\ &\quad - \beta \sum_{l=1}^{k} q_l\left[\frac{1}{6}(\Omega^{k-l+1} e^{-j\varepsilon h} - 2\Omega^{k-l} e^{-j\varepsilon h} + \Omega^{k-l-1} e^{-j\varepsilon h})\right. \\ &\quad + \frac{4}{6}(\Omega^{k-l+1} - 2\Omega^{k-l} + \Omega^{k-l-1}) \\ &\quad \left. + \frac{1}{6}(\Omega^{k-l+1} e^{j\varepsilon h} - 2\Omega^{k-l} e^{j\varepsilon h} + \Omega^{k-l-1} e^{j\varepsilon h})\right], \end{aligned} \tag{5.6}$$

simplifying and using $e^{j\varepsilon h} + e^{-j\varepsilon h} = 2\mathrm{Cos}(\varepsilon h)$, Eq. (5.6) becomes

$$\begin{aligned} \Omega^{k+1} = \frac{1}{\eta}\Bigg[&2\Omega^k - \Omega^{k-1} - \frac{1}{E_1}\sum_{l=1}^{k} q_l(\Omega^{k-l+1} - 2\Omega^{k-l} \\ &- \Omega^{k-l-1})\Bigg], \end{aligned} \tag{5.7}$$

where $\eta = 1 + \frac{\mu_2}{\beta E_1} + \frac{12\mu_1 \mathrm{Sin}^2\frac{\varepsilon h}{2}}{\beta E_1 h^2 (2\mathrm{Sin}^2\frac{\varepsilon h}{2} - 3)}$. It is conform that $\eta \geq 1$ and $E_1 > 0$.

Lemma 5.1. *If Ω^k is the solution for Eq.* (5.7)*, then $|\Omega^k| \leq |\Omega^0|$, $k = 0, 1, 2, \ldots, K$.*

Proof. Mathematical induction is used to show for $k = 0$ Eq. (5.7) becomes

$$|\Omega^1| = \frac{1}{\eta}|\Omega^0| \leq |\Omega^0|, \quad \eta \geq 1.$$

Let us suppose $|\Omega^k| \leq |\Omega^0|$ for $k = 1, 2, \ldots, K-1$, then

$$\begin{aligned} |\Omega^{k+1}| &\leq \frac{1}{\eta}\Bigg[2|\Omega^k| - |\Omega^{k-1}| - \frac{1}{E_1}\sum_{l=1}^{k} q_l(|\Omega^{k-l+1}| - 2|\Omega^{k-l}| \\ &\quad - |\Omega^{k-l-1}|)\Bigg], \\ &\leq \frac{1}{\eta}\left[2|\Omega^0| - |\Omega^0| - \frac{1}{E_1}\sum_{l=1}^{k} q_l(|\Omega^0| - 2|\Omega^0| - |\Omega^0|)\right], \\ &\leq |\Omega^0|. \end{aligned}$$

□

Theorem 1. *Scheme* (3.8) *is unconditionally stable.*

Proof. By employing expression (5.4) and Lemma 5.1, we obtain

$$\|\varrho^k\|_2 \leq \|\varrho^0\|_2, \quad k = 0, 1, \ldots, K.$$

Thus, the presented scheme is unconditionally stable. □

6 Convergence

The convergence of the specific problem will be covered in this part, which is followed by Kadalbajoo *et al*'s. technique [48]. First, the following theorem is promoted [43,49].

Theorem 2. *Suppose that $f(y, s)$ and $U(y, s)$ belong to $C^2(\mathfrak{a}, \mathfrak{b})$ and $C^4(\mathfrak{a}, \mathfrak{b})$, respectively. The equidistance partition of $[\mathfrak{a}, \mathfrak{b}]$ has a step size of h is $\varphi = [\mathfrak{a} = y_0, y_1, y_2, \ldots, y_{\mathcal{N}} = \mathfrak{b}]$ such that $y_\ell - \mathfrak{a} = \ell h$, $\ell = 0, 1, 2, \ldots, \mathcal{N}$. If the unique spline interpolation in our*

problem is $\hat{u}$ at knots $y_0, y_1, y_2, \ldots, y_{\mathcal{N}} \in \varphi$, then there be a constant ζ_i independent of h, then for every $s \geq 0$, we obtain

$$\|\mathfrak{D}^i(U(y,s) - \hat{u}(y,s))\| \leq \zeta_i h^{4-i}, \; i = 0, 1, 2. \tag{6.1}$$

Lemma 6.1. *The CBS set $G_{-1}, G_0, G_1, \ldots, G_{\mathcal{N}+1}$ in Eq. (2.2) satisfies the inequality*

$$\sum_{i=-1}^{\mathcal{N}+1} |G_i(y)| \leq \frac{5}{3}, \; 0 \leq y \leq 1.$$

Theorem 3. *There is a computational approximation $u(y,s)$ to the analytical solution $U(y,s)$ of our problem. Moreover, if $f \in C^2[\mathfrak{a}, \mathfrak{b}]$, then*

$$\|U(y,s) - u(y,s)\|_\infty \leq \tilde{\zeta} h^2, \quad \forall s \geq 0,$$

where h is relatively small and $\tilde{\zeta} > 0$ is free of h.

Proof. Let us assume that $u(y,s)$ is approximated as $\hat{u}(y,s) = \sum_{i=-1}^{\mathcal{N}+1} \Lambda_i^k(s) G_i(y)$. From the triangular inequality, we obtain

$$\|U(y,s) - u(y,s)\|_\infty \leq \|U(y,s) - \hat{u}(y,s)\|_\infty + \|\hat{u}(y,s) - u(y,s)\|_\infty.$$

Using Theorem 2, we obtain

$$\|U(y,s) - u(y,s)\|_\infty \leq \zeta_0 h^4 + \|\hat{u}(y,s) - u(y,s)\|_\infty. \tag{6.2}$$

The proposed scheme has collocation conditions as $LU(y_i, s) = Lu(y_i, s) = f(y_i, s)$, $i = 0(1)\mathcal{N}$. Suppose that $L\hat{u}_1(y,s) = \hat{f}(y_i, s)$, $i = 0(1)\mathcal{N}$.

Thus, for any time stage, the difference $\hat{u}_1(y_i, s) - u(y_i, s)$ for $\theta = 1$ in linear form can be given as

$$\begin{aligned}
&\left[\frac{1}{6}(\beta E_1 + \mu_2) + \frac{\mu_1}{h^2}\right]\Phi_{i-1}^{k+1} \\
&\quad + \left[\frac{4}{6}(\beta E_1 + \mu_2) - \frac{2\mu_1}{h^2}\right]\Phi_i^{k+1} \\
&\quad + \left[\frac{1}{6}(\beta E_1 + \mu_2) + \frac{\mu_1}{h^2}\right]\Phi_{i+1}^{k+1} \\
&= 2\beta E_1\left(\frac{1}{6}\Phi_{i-1}^k + \frac{4}{6}\Phi_i^k + \frac{1}{6}\Phi_{i+1}^k\right) \\
&\quad - \beta E_1\left(\frac{1}{6}\Phi_{i-1}^{k-1} + \frac{4}{6}\Phi_i^{k-1} + \frac{1}{6}\Phi_{i+1}^{k-1}\right) \\
&\quad - \beta \sum_{l=1}^{k} q_l\left[\frac{1}{6}(\Phi_{i-1}^{k-l+1} - 2\Phi_{i-1}^{k-l} + \Phi_{i-1}^{k-l-1})\right. \\
&\quad + \frac{4}{6}(\Phi_i^{k-l+1} - 2\Phi_i^{k-l} + \Phi_i^{k-l-1}) \\
&\quad \left. + \frac{1}{6}(\Phi_{i+1}^{k-l+1} - 2\Phi_{i+1}^{k-l} + \Phi_{i+1}^{k-l-1})\right] + \frac{\mathfrak{R}_i^{k+1}}{h^2},
\end{aligned} \tag{6.3}$$

BCs can be set out as

$$\frac{1}{6}\Phi_{i-1}^{k+1} + \frac{4}{6}\Phi_i^{k+1} + \frac{1}{6}\Phi_{i+1}^{k+1} = 0, \quad i = 0, \mathcal{N},$$

where

$$\Phi_i^k = y_i^k - \psi_i^k, \; i = -1, 0, \ldots, \mathcal{N} + 1$$

and

$$\mathfrak{R}_i^k = h^2[f_i^k - \tilde{f}_i^k], \; i = 0, 1, \ldots, \mathcal{N}.$$

From inequality (6.1), it is clear that

$$|\mathfrak{R}_i^k| = h^2|f_i^k - \tilde{f}_i^k| \leq \zeta h^4.$$

Define $\mathfrak{R}^k = \max\{|\mathfrak{R}_i^k|; 0 \leq i \leq \mathcal{N}\}$, $\varsigma_i^k = |\Phi_i^k|$ and $\varsigma^k = \max\{|\varsigma_i^k|; 0 \leq i \leq \mathcal{N}\}$. When $k = 0$ our Eq. (6.3) becomes

$$\begin{aligned}
&\left[\frac{1}{6}(\beta E_1 + \mu_2) + \frac{\mu_1}{h^2}\right]\Phi_{i-1}^1 \\
&\quad + \left[\frac{4}{6}(\beta E_1 + \mu_2) - \frac{2\mu_1}{h^2}\right]\Phi_i^1 \\
&\quad + \left[\frac{1}{6}(\beta E_1 + \mu_2) + \frac{\mu_1}{h^2}\right]\Phi_{i+1}^1 \\
&= 2\beta E_1\left(\frac{1}{6}\Phi_{i-1}^0 + \frac{4}{6}\Phi_i^0 + \frac{1}{6}\Phi_{i+1}^0\right) + \frac{\mathfrak{R}_i^1}{h^2},
\end{aligned}$$

from ICs we have $\varsigma^0 = 0$ and $i = 0, 1, \ldots, \mathcal{N}$

$$\begin{aligned}
&\left[\frac{4}{6}(\beta E_1 + \mu_2) - \frac{2\mu_1}{h^2}\right]\Phi_i^1 \\
&= -\left[\frac{1}{6}(\beta E_1 + \mu_2) + \frac{\mu_1}{h^2}\right](\Phi_{i-1}^1 + \Phi_{i+1}^1) + \frac{\mathfrak{R}_i^1}{h^2},
\end{aligned}$$

taking suitably small mesh spacing h and norms of $\mathfrak{R}_i^1, \Phi_i^1$ we have

$$\varsigma_i^1 \leq \frac{3\zeta h^4}{h^2(\beta E_1 + \mu_2) - 12\mu_1},$$

from BCs ς_{-1}^1 and $\varsigma_{\mathcal{N}+1}^1$ can be found as

$$\varsigma_{-1}^1 \leq \frac{15\zeta h^4}{h^2(\beta E_1 + \mu_2) - 12\mu_1},$$

$$\varsigma_{\mathcal{N}+1}^1 \leq \frac{15\zeta h^4}{h^2(\beta E_1 + \mu_2) - 12\mu_1},$$

from above results, it is carried out that $\varsigma^1 \leq \zeta_1 h^2$, where ζ_1 is not depending on h. To prove this theorem, mathematical induction is applied to k. Suppose that $\varsigma_i^i \leq \zeta_i h^2$ is true for $i = 1(2)k$ and $\zeta = \max\{\zeta_i : i = 0, 1, 2, \ldots, k\}$, then from Eq. (6.3), we obtain

$$
\begin{aligned}
&\left[\frac{1}{6}(\beta E_1+\mu_2)+\frac{\mu_1}{h^2}\right]\Phi_{\iota-1}^{k+1}\\
&\quad+\left[\frac{4}{6}(\beta E_1+\mu_2)-\frac{2\mu_1}{h^2}\right]\Phi_{\iota}^{k+1}\\
&\quad+\left[\frac{1}{6}(\beta E_1+\mu_2)+\frac{\mu_1}{h^2}\right]\Phi_{\iota+1}^{k+1}\\
&=2\beta E_1\left(\frac{1}{6}\Phi_{\iota-1}^{k}+\frac{4}{6}\Phi_{\iota}^{k}+\frac{1}{6}\Phi_{\iota+1}^{k}\right)\\
&\quad-\left(\frac{1}{6}\Phi_{\iota-1}^{k-1}+\frac{4}{6}\Phi_{\iota}^{k-1}+\frac{1}{6}\Phi_{\iota+1}^{k-1}\right)\beta(q_0-2q_1+q_2)\\
&\quad-\left(\frac{1}{6}\Phi_{\iota-1}^{k-2}+\frac{4}{6}\Phi_{\iota}^{k-2}+\frac{1}{6}\Phi_{\iota+1}^{k-2}\right)\beta(q_1-2q_2+q_3)\\
&\quad-\left(\frac{1}{6}\Phi_{\iota-1}^{k-3}+\frac{4}{6}\Phi_{\iota}^{k-3}+\frac{1}{6}\Phi_{\iota+1}^{k-3}\right)\beta(q_2-2q_3+q_4)\\
&\quad-\ \ldots-\left(\frac{1}{6}\Phi_{\iota-1}^{2}+\frac{4}{6}\Phi_{\iota}^{2}+\frac{1}{6}\Phi_{\iota+1}^{2}\right)\beta(q_{k-3}-2q_{k-2}\\
&\quad+q_{k-1})-\left(\frac{1}{6}\Phi_{\iota-1}^{1}+\frac{4}{6}\Phi_{\iota}^{1}+\frac{1}{6}\Phi_{\iota+1}^{1}\right)\beta(q_{k-2}-2q_{k-1}\\
&\quad+q_k)-\beta q_{k-1}\left(\frac{1}{6}\Phi_{\iota-1}^{0}+\frac{4}{6}\Phi_{\iota}^{0}+\frac{1}{6}\Phi_{\iota+1}^{0}\right)\\
&\quad-2\beta q_k\left(\frac{1}{6}\Phi_{\iota-1}^{0}+\frac{4}{6}\Phi_{\iota}^{0}+\frac{1}{6}\Phi_{\iota+1}^{0}\right)\\
&\quad+\beta q_k\left(\frac{1}{6}\Phi_{\iota-1}^{-1}+\frac{4}{6}\Phi_{\iota}^{-1}+\frac{1}{6}\Phi_{\iota+1}^{-1}\right)+\frac{\Re_{\iota}^{k+1}}{h^2},
\end{aligned}
\tag{6.4}
$$

Eq. (6.4) becomes after applying the norm once again to Φ_{ι}^{k+1} and $\Re_{\iota}^{k+1}$.

$$
\begin{aligned}
\varsigma_{\iota}^{k+1}&\le\frac{3\zeta h^4}{h^2(\beta E_1+\mu_2)-12\mu_1}\\
&\quad\times\left(1+2\beta E_1-\beta\sum_{l=1}^{k-1}(q_{l+1}-2q_l+q_{l-1})\right).
\end{aligned}
$$

Similarly, from BCs, ς_{-1}^{k+1} and $\varsigma_{\mathcal{N}+1}^{k+1}$ can be found out as

$$
\begin{aligned}
\varsigma_{-1}^{k+1}&\le\frac{15\zeta h^4}{h^2(\beta E_1+\mu_2)-12\mu_1}\left(1+2\beta E_1\right.\\
&\quad\left.-\beta\sum_{l=1}^{k-1}(q_{l+1}-2q_l+q_{l-1})\right),\\
\varsigma_{\mathcal{N}+1}^{k+1}&\le\frac{15\zeta h^4}{h^2(\beta E_1+\mu_2)-12\mu_1}\left(1+2\beta E_1\right.\\
&\quad\left.-\beta\sum_{l=1}^{k-1}(q_{l+1}-2q_l+q_{l-1})\right).
\end{aligned}
$$

For all m, we obtain that

$$
\varsigma^{k+1}\le\zeta h^2,
\tag{6.5}
$$

Particularly,

$$
\hat{u}(y,s)-u(y,s)=\sum_{\iota=-1}^{\mathcal{N}+1}(\Lambda_{\iota}(s)-\psi_{\iota}(s))G_{\iota}(y).
$$

Therefore, from inequality (6.5) and Lemma 6.1, we acquire

$$
\|\hat{u}(y,s)-u(y,s)\|_{\infty}\le\frac{5}{3}\zeta h^2.
\tag{6.6}
$$

From inequalities (6.6) and (6.2),

$$
\|U(y,s)-u(y,s)\|_{\infty}\le\zeta_0 h^4+\frac{5}{3}\zeta h^2=\tilde{\zeta}h^2,
$$

where . □

Theorem 4. *The TFKGE is convergent with ICs and BCs.*

Proof. Consider TFKGE has exact solution $U(y,s)$ and approximate solution $u(y,s)$. Therefore, the previous theorem and Eq. (3.3) validate that

$$
\|U(y,s)-u(y,s)\|_{\infty}\le\tilde{\zeta}h^2+\Upsilon(\Delta s)^2.
$$

Here, $\tilde{\zeta}$ and Υ are arbitrary constants. Consequently, in both the spatial and temporal directions, the aforementioned scheme is second-order convergent. □

7 Numerical outcomes and discussion

Some examples of nonlinear TFKGE are discussed in this equation. The effectiveness and precision of this approach will be evaluated by examining the outcomes for various parameter values. Tables and figures that highlight the importance of exact numerical solutions are provided. The method's accuracy has been demonstrated by the computation of the error norms $L_2(\mathcal{N})$ and $L_{\infty}(\mathcal{N})$

$$
\begin{aligned}
L_2(U)&=\|U(y_{\iota},s)-u(y_{\iota},s)\|_2\\
&=\sqrt{h\sum_{\iota=0}^{\mathcal{N}}|U(y_{\iota},s)-u(y_{\iota},s)|^2},\\
L_{\infty}(U)&=\|U(y_{\iota},s)-u(y_{\iota},s)\|_{\infty}\\
&=\max_{0\le\iota\le\mathcal{N}}|U(y_{\iota},s)-u(y_{\iota},s)|.
\end{aligned}
$$

This problem's order of convergence is determined using the formula found in [50]

$$
\log_2\left(\frac{L_{\infty}(\mathcal{N})}{L_{\infty}(2\mathcal{N})}\right).
$$

Table 1: Absolute error for $\alpha = 1.9$, $\Delta s = 6.66667 \times 10^{-5}$, and $\mathcal{N} = 200$ of Example 7.1 at $s = 0.1$

y	Exact	Approximate	Absolute error
0.1	−0.0278115294	−0.0278114929	$3.656752743 \times 10^{-8}$
0.2	−0.0529006727	−0.0529005974	$7.527881930 \times 10^{-8}$
0.3	−0.0728115294	−0.0728114184	$1.110329535 \times 10^{-7}$
0.4	−0.0855950864	−0.0855949500	$1.364560458 \times 10^{-7}$
0.5	−0.09	−0.0899998543	$1.456675959 \times 10^{-7}$
0.6	−0.0855950864	−0.0855949500	$1.364560391 \times 10^{-7}$
0.7	−0.0728115294	−0.0728114184	$1.110329550 \times 10^{-7}$
0.8	−0.0529006727	−0.0529005974	$7.527881830 \times 10^{-8}$
0.9	−0.0278115294	−0.0278114929	$3.656752227 \times 10^{-8}$

For all cases, the normalization function is assumed to be $AB(\alpha) = 1$. Numerical calculations are carried out by utilizing Mathematica 13.2 for numerical calculations on an Intel(R)Core(TM) i5-3437U Central Processing Unit (CPU) @2.60 GHz, 2,712 MHz with 16 GB RAM, SSD and 64-bit operating system (Windows 11 pro). CPU takes a few seconds to complete the numerical simulation for the obtained results tabulated in Tables.

Example 7.1. Eq. (1.1) takes the form

$$\frac{\partial^{\alpha} U(y,s)}{\partial s^{\alpha}} - \frac{\partial^2 U(y,s)}{\partial y^2} + U^2(y,s) = f(y,s), s \in [0,T], y \in [\mathfrak{a},\mathfrak{b}], 1 < \alpha \le 2,$$

when $\mu_1 = -1$, $\mu_2 = 0$, $\mu_3 = 1$, and $\sigma = 2$. with ICs

$$U(y,0) = 0, U_s(y,0) = -\mathrm{Sin}(\pi y),$$

and BCs

$$U(0,s) = 0, U(1,s) = 0.$$

The source term on the right-hand side for $AB(\alpha) = 1$ is

$$\pi^2(s^2 - s)\,\mathrm{Sin}(\pi y) + (s^2 - s)^2 \mathrm{Sin}^2(\pi y) + \frac{1}{2-\alpha} 2s\,\mathrm{Sin}(\pi y) E_{\alpha,2}\left[\frac{-\alpha}{2-\alpha} s^{\alpha}\right].$$

The exact solution is $(s^2 - s)\,\mathrm{Sin}(\pi y)$.

Table 3: Order of convergence and CPU time in seconds for Example 7.1 by taking various values of h when $\Delta s = \frac{1}{K}$, $s = 0.2$, and $K = 500$

α	h	$L_{\infty}(\mathcal{N})$	$L_2(\mathcal{N})$	Order	CPU time (s)
1.3	$\frac{1}{2}$	1.6371623×10^{-2}	115764859×10^{-2}	...	0.346
	$\frac{1}{4}$	4.2262794×10^{-3}	2.9874036×10^{-3}	1.953737324	0.454
	$\frac{1}{8}$	1.0613170×10^{-3}	7.5004257×10^{-4}	1.993532400	0.797
	$\frac{1}{16}$	2.6847775×10^{-4}	1.8965561×10^{-4}	1.982981316	1.188
1.5	$\frac{1}{2}$	1.3289605×10^{-2}	9.3971704×10^{-3}	...	0.347
	$\frac{1}{4}$	3.3820259×10^{-3}	2.3906596×10^{-3}	1.974338701	0.455
	$\frac{1}{8}$	8.4622189×10^{-4}	5.9803402×10^{-4}	1.998779789	0.797
	$\frac{1}{16}$	2.1391493×10^{-4}	1.5109849×10^{-4}	1.983998831	1.189
1.7	$\frac{1}{2}$	9.2073906×10^{-3}	6.5106083×10^{-3}	...	0.348
	$\frac{1}{4}$	2.3047006×10^{-3}	1.6291675×10^{-3}	1.998213010	0.456
	$\frac{1}{8}$	5.7428612×10^{-4}	4.0585304×10^{-4}	2.004737736	0.797
	$\frac{1}{16}$	1.4507002×10^{-4}	1.0244950×10^{-4}	1.985020278	1.190
1.9	$\frac{1}{2}$	3.7158149×10^{-3}	2.6274779×10^{-3}	...	0.347
	$\frac{1}{4}$	9.1243828×10^{-4}	6.4503341×10^{-4}	2.025879777	0.456
	$\frac{1}{8}$	2.2631463×10^{-4}	1.5993108×10^{-4}	2.011397104	0.797
	$\frac{1}{16}$	5.7147116×10^{-5}	4.0331656×10^{-5}	1.985577267	1.188

The exact and approximate solutions with absolute error when $\alpha = 1.9$, $\Delta s = 6.66667 \times 10^{-5}$, $\mathcal{N} = 200$, and $s = 0.1$ are displayed in Table 1. Table 2 shows the comparison of error norm at different time intervals. The order of convergence and CPU time(s) for distinct values of h is demonstrated in Table 3. The order of convergence, CPU time(s), and error norm are shown in Table 4, when $\mathcal{N} = K$ and $s = 0.5$. Figure 1 displays a very perfect agreement of exact and spline solutions at different time levels with fixed $K = 500$, when $\mathcal{N} = 200$, 250, and $\alpha = 1.5$, 1.8. Figure 2 shows the exact and approximate answers plotted in three dimensions when $\mathcal{N} = 150$, $\alpha = 1.8$, $\Delta s = 0.0002$, and $s = 0.1$. The 3D interpretation of absolute computational

Table 2: Error norms at various time stages for different values of α, where $K = 1{,}000$ and $\mathcal{N} = 250$ of Example 7.1

	$L_{\infty}(\mathcal{N})$			$L_2(\mathcal{N})$		
s	$\alpha = 1.4$	$\alpha = 1.6$	$\alpha = 1.8$	$\alpha = 1.4$	$\alpha = 1.6$	$\alpha = 1.8$
0.1	6.73839×10^{-7}	4.81267×10^{-7}	2.61254×10^{-7}	4.60672×10^{-7}	3.26135×10^{-7}	1.74347×10^{-7}
0.3	5.81984×10^{-6}	4.72019×10^{-6}	3.03288×10^{-6}	4.04298×10^{-6}	3.26403×10^{-6}	2.06847×10^{-6}
0.5	8.56308×10^{-6}	8.53922×10^{-6}	7.24638×10^{-6}	6.03528×10^{-6}	6.00963×10^{-6}	5.06737×10^{-6}
0.7	1.97375×10^{-6}	5.52719×10^{-6}	9.29263×10^{-6}	1.54532×10^{-6}	4.04468×10^{-6}	6.67782×10^{-6}
0.9	8.66438×10^{-6}	3.07915×10^{-6}	7.29241×10^{-6}	5.93648×10^{-6}	1.98424×10^{-6}	5.40353×10^{-6}

Table 4: Comparison of error norm, order of convergence, and CPU time (s) for Example 7.1 with different values of K, when $s = 0.5$

α	$\mathcal{N} = K$	$L_\infty(\mathcal{N})$	$L_2(\mathcal{N})$	Order	CPU time (s)
1.1	5	7.4808851×10^{-3}	5.5567089×10^{-3}	...	0.125
	10	2.3244434×10^{-3}	1.6403071×10^{-3}	1.686323685	0.210
	20	7.1210012×10^{-4}	5.0237068×10^{-4}	1.706733288	0.365
	40	2.3614005×10^{-4}	1.6654398×10^{-4}	1.592437307	0.476
1.2	5	7.3983654×10^{-3}	5.4953510×10^{-3}	...	0.125
	10	2.3197056×10^{-3}	1.6368747×10^{-3}	1.673264824	0.211
	20	7.1963335×10^{-4}	5.0763330×10^{-4}	1.688607772	0.366
	40	2.4242026×10^{-4}	1.7094775×10^{-4}	1.569751743	0.476
1.3	5	7.2748488×10^{-3}	5.4035065×10^{-3}	...	0.126
	10	2.3013032×10^{-3}	1.6237576×10^{-3}	1.660466191	0.210
	20	7.2311238×10^{-4}	5.1001250×10^{-4}	1.670159293	0.365
	40	2.4749960×10^{-4}	1.7449289×10^{-4}	1.546793666	0.477
1.4	5	7.0960288×10^{-3}	5.2705303×10^{-3}	...	0.126
	10	2.2634463×10^{-3}	1.5968470×10^{-3}	1.648490759	0.211
	20	7.2034058×10^{-4}	5.0794584×10^{-4}	1.651770009	0.366
	40	2.5049972×10^{-4}	1.7655337×10^{-4}	1.523870192	0.476

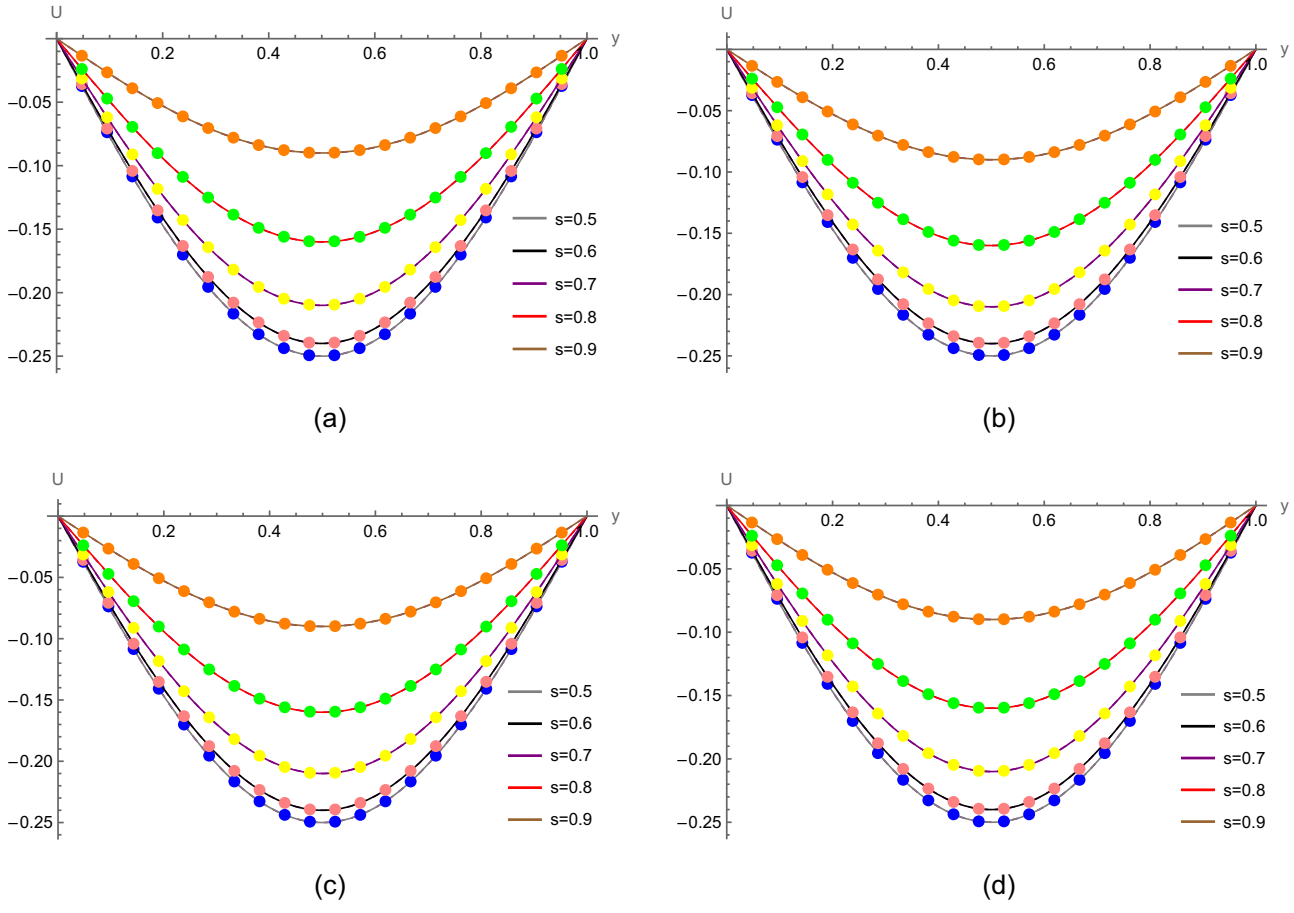

Figure 1: Exact and numerical solutions for Example 7.1 at different time stages. (a) $\mathcal{N} = 200; \alpha = 1.5, K = 500$; (b) $\mathcal{N} = 200, \alpha = 1.8, K = 500$; (c) $\mathcal{N} = 250, \alpha = 1.5, K = 500$; and (d) $\mathcal{N} = 250, \alpha = 1.8, K = 500$.

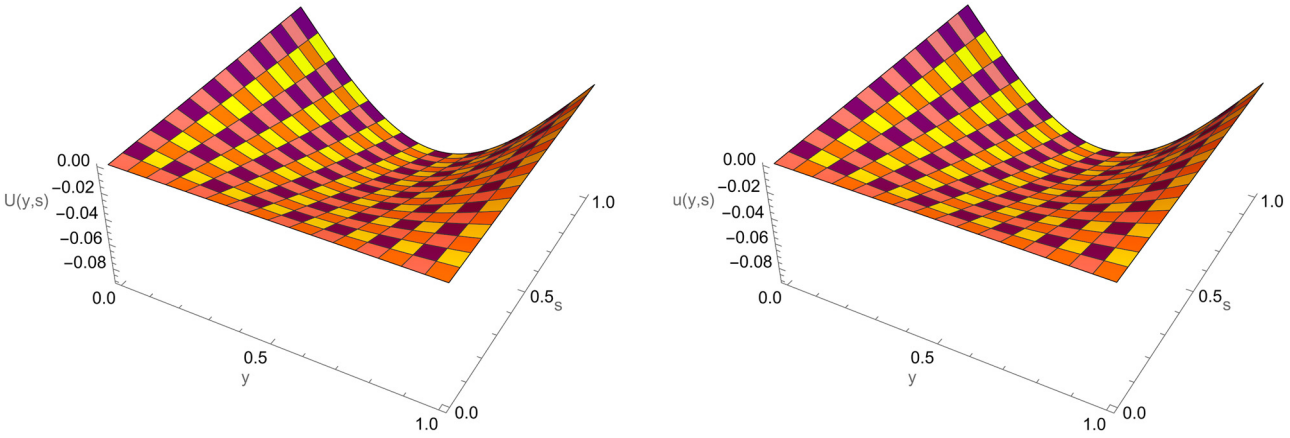

(a) (b)

Figure 2: 3D (a) exact and (b) approximate solution for Example 7.1, when $\mathcal{N} = 150$, $\alpha = 1.8$, $\Delta s = 0.0002$, and $s = 0.1$.

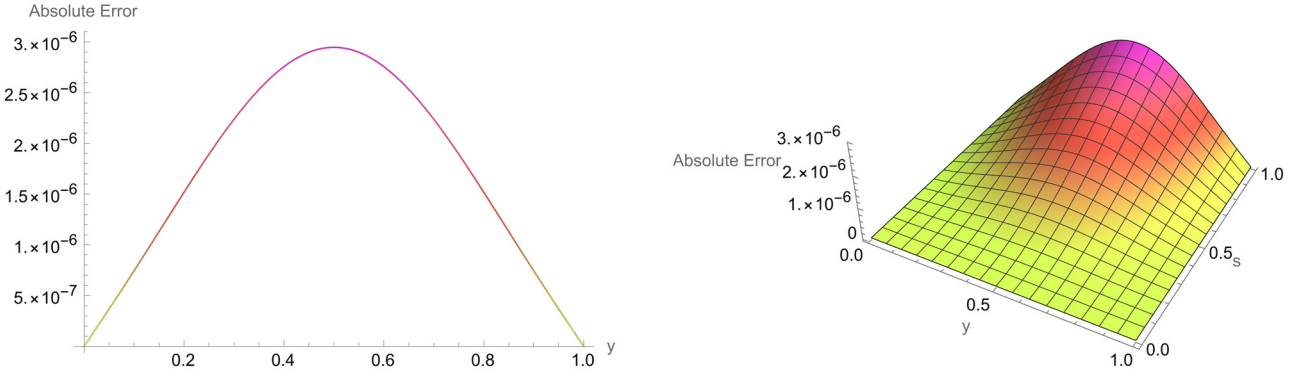

(a) (b)

Figure 3: (a) 2D and (b) 3D error profiles for Example 7.1, when $\mathcal{N} = 250$, $\alpha = 1.7$, $\Delta s = 0.0004$, and $s = 0.2$.

errors at each time and space levels when $s = 0.2$ is shown in Figure 3 corresponding to fixed values of $\mathcal{N}$ and Δs. As the time steps obtain smaller, the numerical model approaches the real-world system more closely. Error diminishes as the value of α increases. This model accurately depicts the physical behavior of that field under realistic conditions. Theoretically order of convergence is 2 and the numerical order of convergence becomes close to 2, which is excellent.

Example 7.2. Eq. (1.1) becomes

$$\frac{\partial^{\alpha} U(y,s)}{\partial s^{\alpha}} - \frac{\partial^2 U(y,s)}{\partial y^2} + U(y,s) - \frac{5}{2}U^3(y,s) = f(y,s), s \in [0,T], y \in [\mathfrak{a},\mathfrak{b}], 1 < \alpha \le 2,$$

when $\mu_1 = -1$, $\mu_2 = 1$, $\mu_3 = -\frac{5}{2}$, and $\sigma = 3$. ICs are

$$U(y,0) = 0, U_s(y,0) = 0,$$

and BCs

$$U(0,s) = 0, U(1,s) = s^2 \mathrm{Sin}h[1].$$

The source term on the right-hand side for $AB(\alpha) = 1$ is

$$-\frac{5}{2}s^6 \mathrm{Sin}^3 hy + \frac{1}{2-\alpha} 2s \mathrm{Sin}\, hy E_{\alpha,2}\left[\frac{-\alpha}{2-\alpha}s^{\alpha}\right].$$

The exact solution is $s^2 \mathrm{Sin}\, hy$. The absolute errors are shown in Table 5, when $\Delta s = 0.0002$, $s = 0.02$, $\alpha = 1.9$, and $\mathcal{N} = 200$. The error norm L_{∞}, L_2 of both $U(y,s)$ and $u(y,s)$, for Example 7.2, corresponding to different α, by setting $\mathcal{N} = 250$, $K = 1{,}000$, are listed in Table 6. Convergence and a comparison of the error norm are included in Table 7 for distinct h. The absolute error profile for solutions $U(y,s)$ and $u(y,s)$ at various time intervals and system specifications is shown in Figure 4. Multiple curves at different time levels are provided to illustrate the

Table 5: Absolute error of Example 7.2, when $\Delta s = 0.0002$, $s = 0.02$, $\alpha = 1.9$, and $\mathcal{N} = 200$

y	Exact	Approximate	Absolute error
0.1	0.0040066700	0.0040066699	$6.7842005 \times 10^{-11}$
0.2	0.0080534401	0.0080534399	$1.5687865 \times 10^{-10}$
0.3	0.0121808117	0.0121808114	$2.9037242 \times 10^{-10}$
0.4	0.0164300930	0.0164300925	$4.9589930 \times 10^{-10}$
0.5	0.0208438122	0.0208438114	$8.0781467 \times 10^{-10}$
0.6	0.0254661432	0.0254661420	1.2689799×10^{-9}
0.7	0.0303433480	0.0303433461	1.9234388×10^{-9}
0.8	0.0355242392	0.0355242365	2.7461670×10^{-9}
0.9	0.0410606690	0.0410606658	3.2079126×10^{-9}

compatibility of the exact and approximate solutions. 3D interpretations of exact and approximate solutions are displayed in Figure 5. The plots of absolute computational errors are shown in Figure 6. Similar to previous example, as the time steps become smaller, the numerical solution approaches the exact solution. Error decreases as α grows.

Example 7.3. Eq. (1.1) becomes

$$\frac{\partial^{\alpha} U(y,s)}{\partial s^{\alpha}} - \frac{\partial^2 U(y,s)}{\partial y^2} + U^2(y,s) = f(y,s), \quad s \in [0,T], \quad y \in [\mathfrak{a},\mathfrak{b}], 1 < \alpha \le 2,$$

when $\mu_1 = -1$, $\mu_2 = 0$, $\mu_3 = 1$, and $\sigma = 2$. ICs are

$$U(y,0) = 0, U_s(y,0) = 0,$$

and BCs

$$U(0,s) = s^{3.5}, U(1,s) = 0.$$

The source term on the right-hand side for $AB(\alpha) = 1$ is

$$\frac{\Gamma[3+\alpha]}{2-\alpha} s^{\alpha+1}(1-y)^{\frac{5}{2}} E_{\alpha,2+\alpha}\left[\frac{-\alpha}{2-\alpha} s^{\alpha}\right] - \frac{15}{4} s^{2+\alpha}(1-y)^{\frac{1}{2}} + s^{4+2\alpha}(1-y)^5.$$

Table 7: Comparison of error norm for different choices of h, when $s = 0.2$, $h = \frac{1}{\mathcal{N}}$, $\Delta s = \frac{1}{K}$, and $K = 500$ in Example 7.2

α	$\mathcal{N}$	$L_\infty(\mathcal{N})$	$L_2(\mathcal{N})$	Order
1.6	4	3.7774133×10^{-6}	2.4992255×10^{-6}	...
	8	9.0027649×10^{-7}	6.1340419×10^{-7}	2.068958589
	16	2.3173668×10^{-7}	1.5718756×10^{-7}	1.957881719
	32	6.7324896×10^{-8}	4.4491038×10^{-8}	1.783274428
1.7	4	3.1245615×10^{-6}	2.0036041×10^{-6}	...
	8	7.3540190×10^{-7}	4.9126714×10^{-7}	2.087048932
	16	1.8870828×10^{-7}	1.2580857×10^{-7}	1.962375174
	32	5.4940372×10^{-8}	3.5634125×10^{-8}	1.780219128
1.8	4	2.3456286×10^{-6}	1.4459448×10^{-6}	...
	8	5.4020202×10^{-7}	3.5434888×10^{-7}	2.118403683
	16	1.3801009×10^{-7}	9.0667592×10^{-8}	1.968725266
	32	4.0681177×10^{-8}	2.5715370×10^{-8}	1.762340439
1.9	4	1.3751370×10^{-6}	8.0570457×10^{-7}	...
	8	3.0680787×10^{-7}	1.9793467×10^{-7}	2.164168008
	16	8.0551321×10^{-8}	5.0569659×10^{-8}	1.929355353
	32	2.3809974×10^{-8}	1.4372078×10^{-8}	1.758342193

The exact solution is $s^{2+\alpha}(1-y)^{\frac{5}{2}}$.

The maximum absolute error in the approximations of U and u at time levels $s = 0.1$, with $\Delta s = 0.0004$ and $\mathcal{N} = 50$ is shown in Table 8. The error norms L_∞ and L_2 at $s = 0.2$, 0.4, 0.6, 0.8, 1.0 are shown in Table 9, when $\mathcal{N} = 50$, $\Delta s = 0.0004$. The behavior of numerical solutions with $\alpha = 1.9$, $\mathcal{N} = 50$, and $K = 500$ at various time stages is displayed in Figure 7. A fairly accurate agreement between exact and spline solutions at various time levels with fixed $\mathcal{N} = 50$, $s = 0.1$, and $K = 500$ is shown in Figure 7. Figure 8 displays the numerical and exact solutions in three dimensions, when $\mathcal{N} = 60$, $\alpha = 1.9$, $\Delta s = 0.004$, and $s = 1$. Figure 9 displays the 3D interpretation of the absolute computation errors at each time and space level when $\mathcal{N} = 40$, $\alpha = 1.9$, $\Delta s = 0.0002$, and $s = 0.1$.

Example 7.4. Consider the TFKGE [51,52]

Table 6: Error norms for various choices of α, when $\mathcal{N} = 250$, $K = 1{,}000$, and $y\varepsilon[0,1]$ of Example 7.2

	$L_\infty(\mathcal{N})$			$L_2(\mathcal{N})$		
s	$\alpha = 1.5$	$\alpha = 1.7$	$\alpha = 1.9$	$\alpha = 1.5$	$\alpha = 1.7$	$\alpha = 1.9$
0.2	9.25699×10^{-9}	6.69602×10^{-9}	3.07029×10^{-9}	5.16715×10^{-9}	3.55601×10^{-9}	1.47887×10^{-9}
0.4	8.00555×10^{-7}	6.09058×10^{-7}	3.11032×10^{-7}	4.66141×10^{-7}	3.36743×10^{-7}	1.54869×10^{-7}
0.6	1.12866×10^{-5}	8.86676×10^{-6}	4.91739×10^{-6}	6.84173×10^{-6}	5.11432×10^{-6}	2.55188×10^{-6}
0.8	7.51079×10^{-5}	6.03155×10^{-5}	3.58051×10^{-5}	4.67668×10^{-5}	3.58957×10^{-5}	1.92279×10^{-5}
1.0	3.43036×10^{-4}	2.77837×10^{-4}	1.72767×10^{-4}	2.17271×10^{-4}	1.69112×10^{-4}	9.54866×10^{-5}

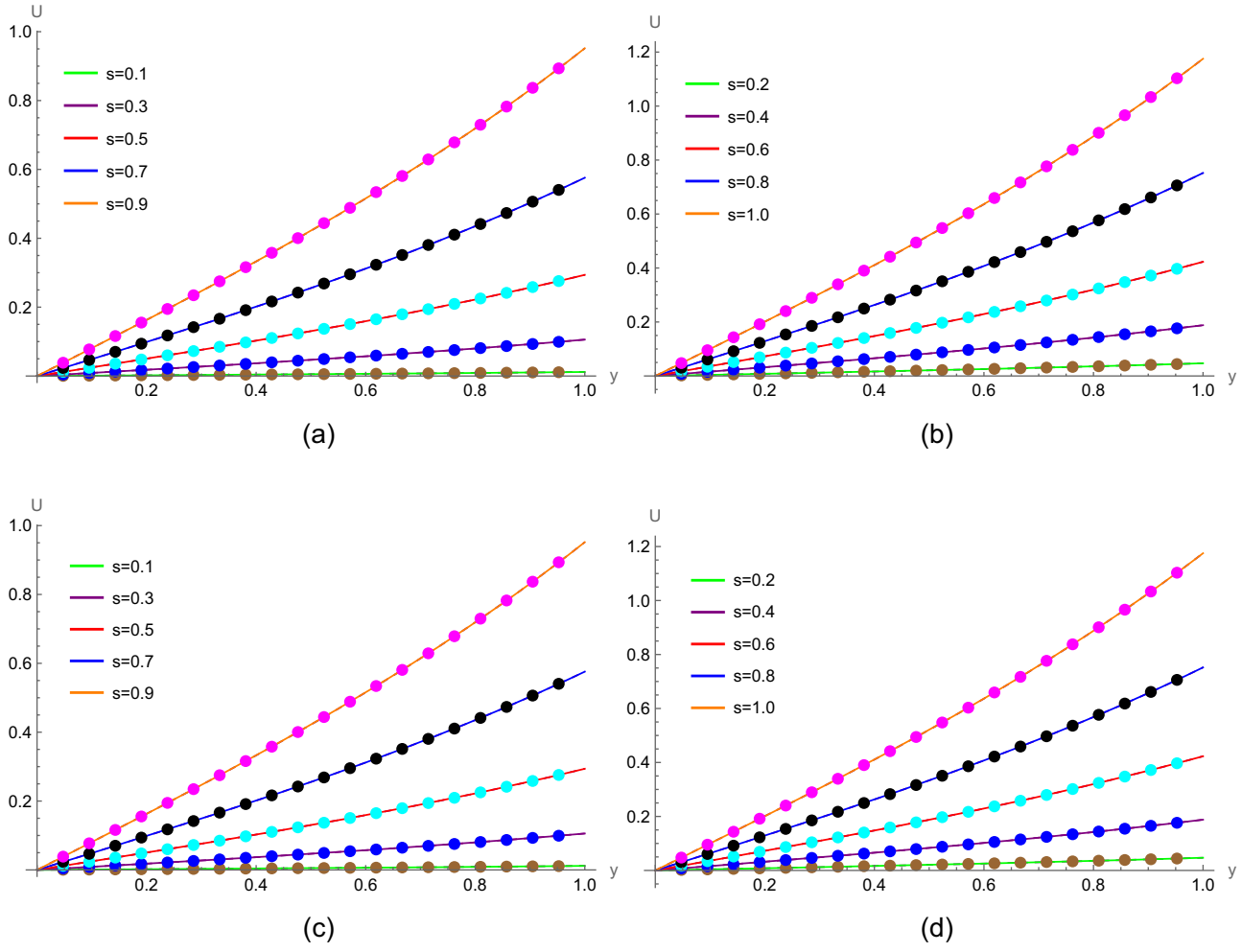

Figure 4: Exact and numerical solutions for Example 7.1 at different time stages. (a) $\mathcal{N} = 200$, $\alpha = 1.6$, $K = 500$; (b) $\mathcal{N} = 200$, $\alpha = 1.6$, $K = 500$; (c) $\mathcal{N} = 250$, $\alpha = 1.9$, $K = 500$; and (d) $\mathcal{N} = 250$, $\alpha = 1.9$, $K = 500$.

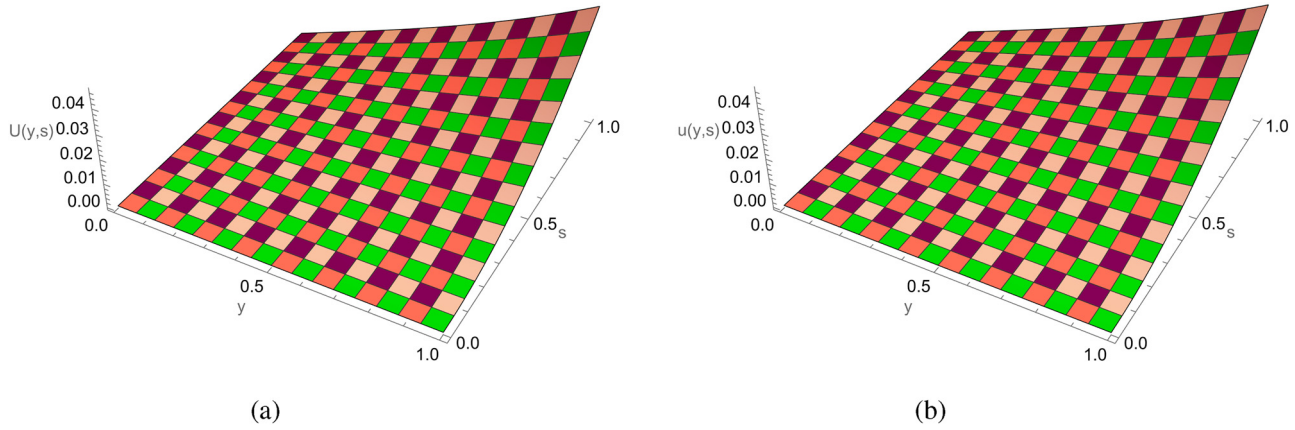

Figure 5: 3D (a) exact and (b) approximate solution for Example 7.1, when $\mathcal{N} = 230$, $\alpha = 1.9$, $\Delta s = 0.0004$, and $s = 0.2$.

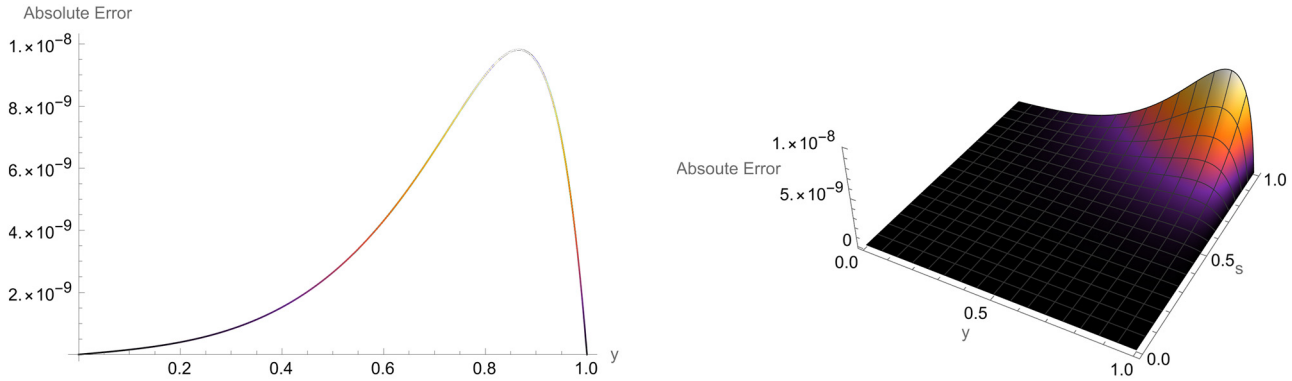

(a) (b)

Figure 6: 2D and 3D error profiles for Example 7.1, when $\mathcal{N} = 220$, $\alpha = 1.8$, $\Delta s = 0.0004$, and $s = 0.2$. (a) 2D error function and (b) 3D error function.

Table 8: Absolute error of Example 7.3 where $\Delta s = 0.0004$, $s = 0.1$, $\alpha = 1.5$, and $\mathcal{N} = 50$

y	Exact	Approximate	Absolute error
0.1	0.0002430000	0.0002437344	7.3449652×10^{-7}
0.2	0.0001810193	0.0001819209	9.0160308×10^{-7}
0.3	0.0001296418	0.0001304546	8.1284947×10^{-7}
0.4	0.0000881816	0.0000888162	6.3458903×10^{-7}
0.5	0.0000559016	0.0000563501	4.4846070×10^{-7}
0.6	0.0000320000	0.0000322898	2.8982447×10^{-7}
0.7	0.0000155884	0.0000157586	1.7017459×10^{-7}
0.8	5.6568542494	5.7458041320	8.8949882×10^{-8}
0.9	1.0000000000	1.0387357529	3.8735752×10^{-8}

$$\frac{\partial^\alpha U(y,s)}{\partial s^\alpha} - \frac{\partial^2 U(y,s)}{\partial y^2} + U(y,s) + \frac{3}{2}U^3(y,s) = f(y,s), s \in [0,T], y \in [\mathfrak{a},\mathfrak{b}], 1 < \alpha \le 2,$$

with ICs

$$U(y,0) = 0, U_s(y,0) = 0,$$

and BCs

$$U(0,s) = 0, U(1,s) = 0.$$

The source term on the right-hand side for $AB(\alpha) = 1$ is

$$\frac{\Gamma[3+\alpha]}{2-\alpha}s^{\alpha+1}\mathrm{Sin}(\pi y)E_{\alpha,2+\alpha}\left[\frac{-\alpha}{2-\alpha}s^\alpha\right] + (\pi^2+1)s^{2+\alpha}\mathrm{Sin}(\pi y) + \frac{3}{2}s^{6+3\alpha}\mathrm{Sin}^3(\pi y).$$

The exact solution is $s^{2+\alpha}\mathrm{Sin}(\pi y)$.

Table 10 shows the absolute numerical errors at various grid points of the CBS solution, with $\mathcal{N} = 100$ and $\Delta s = 0.0001$. Table 11 shows the absolute and relative errors of this problem using the current approach at various time levels, when $\mathcal{N} = 100$, $\Delta s = 0.001$, $s = 0.1$. It is evident that the outcomes are better than those attained by the redefined extended cubic B-spline (RECBS) [30] and Sinc-Chebyshev collocation method (SCCM) [52]. The behavior of exact and numerical solutions, when $\mathcal{N} = 100$, $\alpha = 1.9$, and $K = 500$ at various time stages is displayed in Figure 10. Figure 11 shows the 3D plot of exact and numerical solutions with $\mathcal{N} = 100, \alpha = 1.9, \Delta s = 0.0001$, and $s = 0.1$. Figure 12 shows a visualization of the absolute error between the

Table 9: Error norm of Example 7.3 for multiple choices of α, when $\mathcal{N} = 60$, $K = 250$, and $y\varepsilon[0,1]$

	$L_\infty(\mathcal{N})$			$L_2(\mathcal{N})$		
s	$\alpha = 1.5$	$\alpha = 1.7$	$\alpha = 1.9$	$\alpha = 1.5$	$\alpha = 1.7$	$\alpha = 1.9$
0.2	7.66903×10^{-6}	7.42665×10^{-6}	8.01926×10^{-6}	4.76833×10^{-6}	4.37695×10^{-6}	4.28744×10^{-6}
0.4	5.93395×10^{-5}	7.02222×10^{-5}	9.52235×10^{-5}	3.93501×10^{-5}	4.44089×10^{-5}	5.43930×10^{-5}
0.6	1.83896×10^{-4}	2.44466×10^{-4}	3.75646×10^{-4}	1.25694×10^{-4}	1.61606×10^{-4}	2.26143×10^{-4}
0.8	4.05266×10^{-4}	5.70042×10^{-4}	9.30403×10^{-4}	2.80807×10^{-4}	3.88137×10^{-4}	5.89458×10^{-4}
1.0	8.01692×10^{-4}	1.10532×10^{-3}	1.78722×10^{-3}	5.54959×10^{-4}	7.65002×10^{-4}	1.18938×10^{-3}

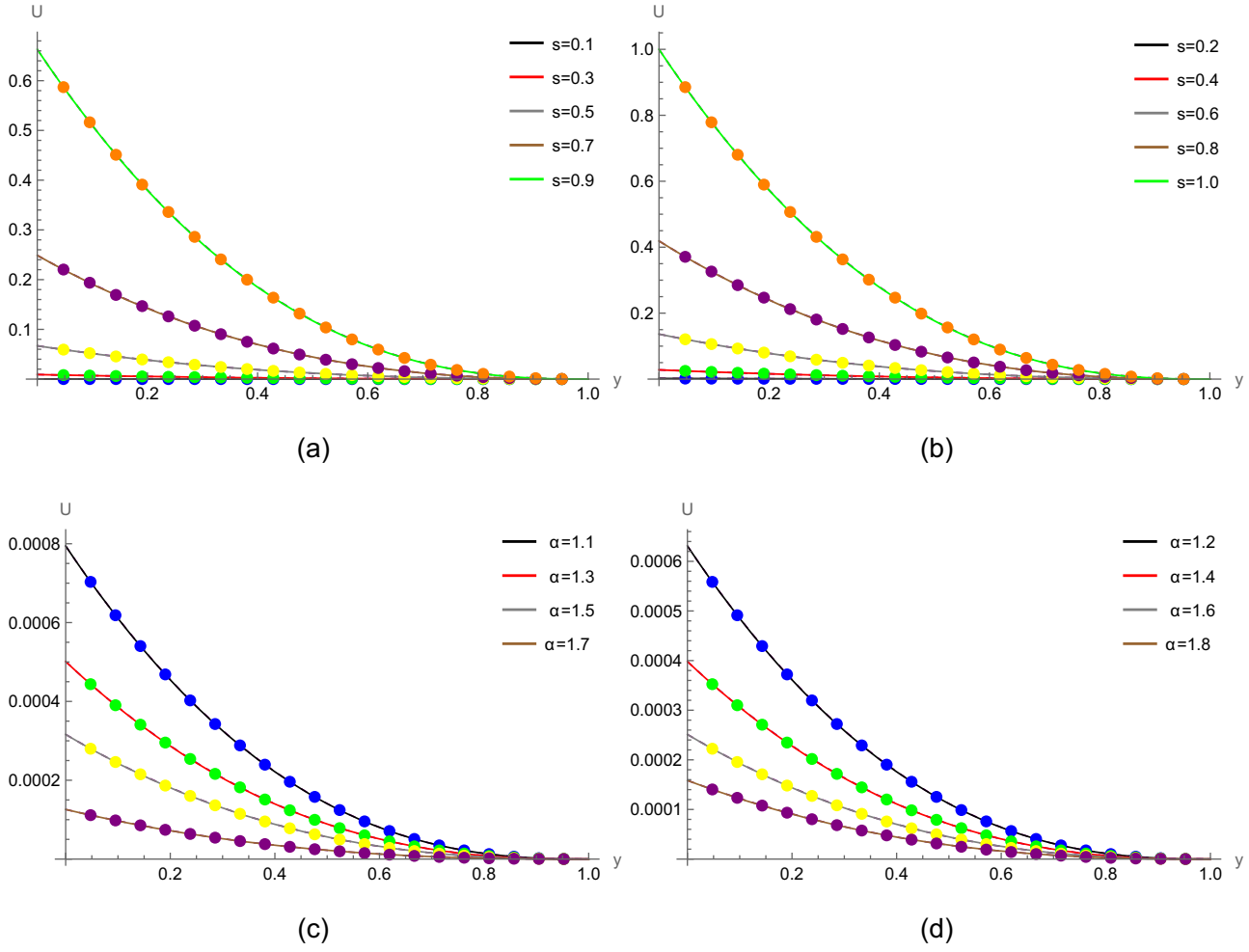

Figure 7: Exact and numerical solutions of Example 7.3 at different time stages. (a) $\mathcal{N} = 50$, $\alpha = 1.9$, $K = 500$, (b) $\mathcal{N} = 50$, $\alpha = 1.9$, $K = 500$, (c) $\mathcal{N} = 50$, $s = 0.1$, $K = 500$, (d) $\mathcal{N} = 50$, $s = 0.1$, $K = 500$.

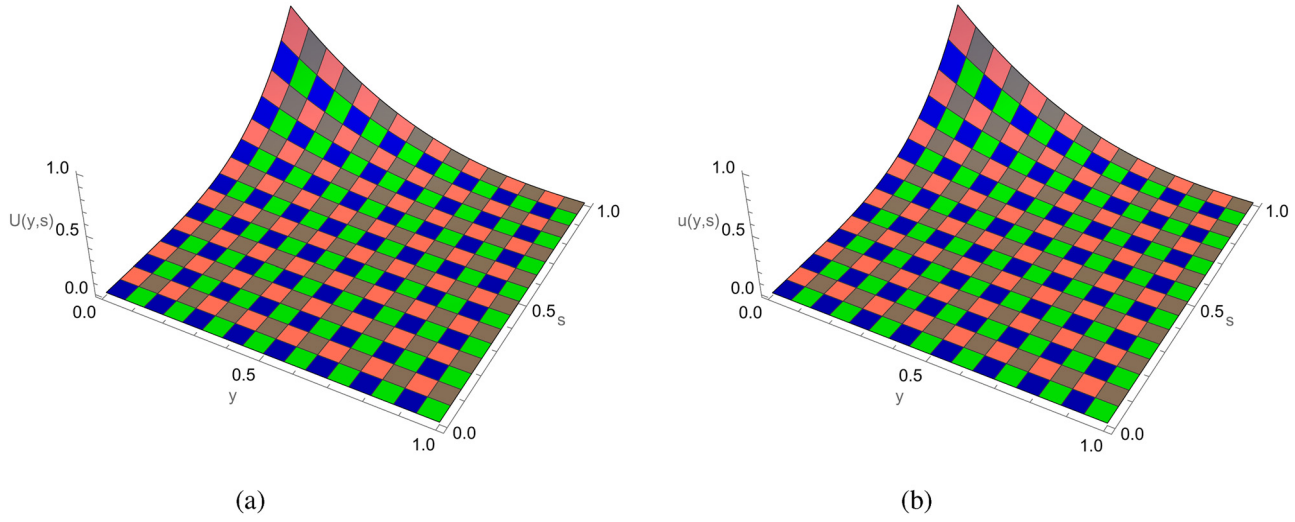

Figure 8: 3D (a) exact and (b) approximate solutions of Example 7.3, when $\mathcal{N} = 60$, $\alpha = 1.9$, $\Delta s = 0.004$, and $s = 1$.

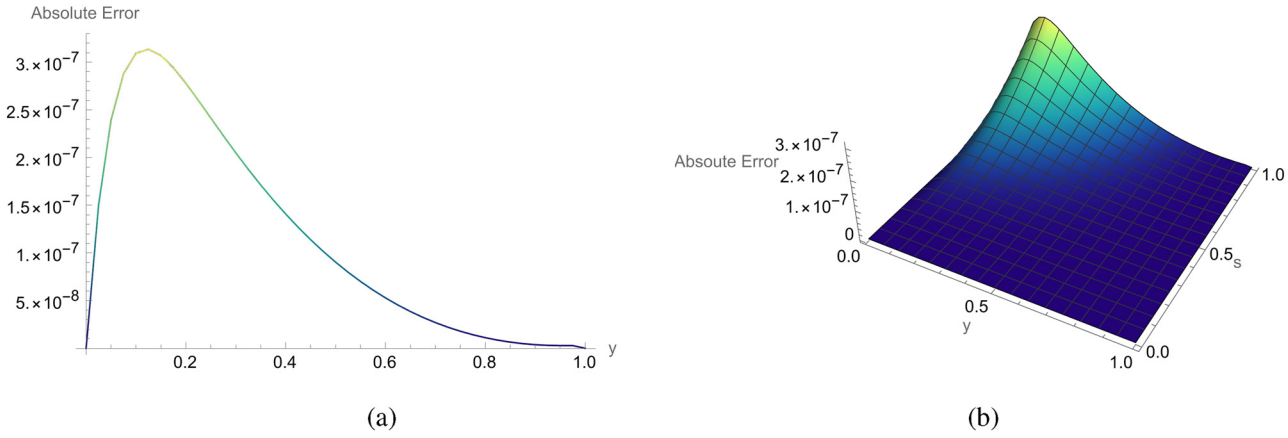

Figure 9: 2D and 3D error profiles of Example 7.3, when $\mathcal{N} = 40$, $\alpha = 1.9$, $\Delta s = 0.0002$, and $s = 0.1$. (a) 2D error function and (b) 3D error function.

Table 10: Absolute error of Example 7.4, when $\Delta s = 0.0001$, $s = 0.1$, $\alpha = 1.9$, and $\mathcal{N} = 100$

y	Exact	Approximate	Absolute error
0.1	0.0000389029	0.0000389766	7.3740138×10^{-8}
0.2	0.0000739977	0.0000741380	1.4026207×10^{-7}
0.3	0.0001018492	0.0001020422	1.9305418×10^{-7}
0.4	0.0001197309	0.0001199578	2.2694881×10^{-7}
0.5	0.0001258925	0.0001261311	2.3862810×10^{-7}
0.6	0.0001197309	0.0001199578	2.2694881×10^{-7}
0.7	0.0001018492	0.0001020422	1.9305418×10^{-7}
0.8	0.0000739977	0.0000741380	1.4026207×10^{-7}
0.9	0.0000389029	0.0000389766	7.3740138×10^{-8}

exact and approximation solutions using $\mathcal{N} = 50$, $\alpha = 1.9$, $\Delta s = 0.0001$, and $s = 0.1$.

8 Concluding remarks

In physics, cosmology, and engineering, the nonlinear TFKGE is an effective tool for simulating memory-dependent, nonlinear, and relativistic wave events. Modern theoretical and applied research requires a deeper knowledge of complex wave dynamics, anomalous transport, and self-interacting fields. The problem of finding a numerical solution for TFKGE involving the ABTFD is the focus of this research. The solution curve was interpolated in the spatial direction using CBS functions, and the finite difference formula was employed to approximate ABTFD. This study's technique is novel and provides an acceptable level of accuracy. This method is reliable as the suggested strategy offers second-order convergence in both the temporal and spatial directions and is unconditionally stable. When applied to numerical applications, the provided approach

Table 11: Error norm of Example 7.4 for multiple choices of α, when $\mathcal{N} = 100$, $\Delta s = 0.001$, $s = 0.1$, and $y\varepsilon[0, 1]$

	SCCM [52]		RECBS [30]		Proposed method	
y	$\alpha = 1.7$	$\alpha = 1.9$	$\alpha = 1.7$	$\alpha = 1.9$	$\alpha = 1.7$	$\alpha = 1.9$
0.1	1.5471×10^{-3}	1.5471×10^{-3}	8.4422×10^{-6}	9.8439×10^{-6}	1.0484×10^{-6}	7.4076×10^{-7}
0.2	1.1272×10^{-3}	9.4914×10^{-4}	1.4959×10^{-7}	6.7965×10^{-6}	1.9941×10^{-6}	1.4090×10^{-6}
0.3	8.9663×10^{-4}	6.7913×10^{-4}	2.7610×10^{-6}	1.0853×10^{-5}	2.7447×10^{-6}	1.9393×10^{-6}
0.4	6.3348×10^{-4}	3.9687×10^{-4}	5.8360×10^{-6}	7.0990×10^{-6}	3.2266×10^{-6}	2.2798×10^{-6}
0.5	5.6868×10^{-4}	3.2651×10^{-4}	7.1727×10^{-6}	3.1898×10^{-5}	3.3927×10^{-6}	2.3971×10^{-6}
0.6	6.3348×10^{-4}	3.9687×10^{-4}	5.8360×10^{-6}	4.1207×10^{-6}	3.2266×10^{-6}	2.2798×10^{-6}
0.7	8.9663×10^{-4}	6.7913×10^{-4}	2.7610×10^{-6}	8.6781×10^{-6}	2.7447×10^{-6}	1.9393×10^{-6}
0.8	1.1272×10^{-3}	9.4914×10^{-4}	1.4959×10^{-7}	6.7965×10^{-6}	1.9941×10^{-6}	1.4090×10^{-6}
0.9	1.5471×10^{-3}	1.4380×10^{-3}	8.4422×10^{-6}	9.8439×10^{-6}	1.0484×10^{-6}	7.4076×10^{-7}

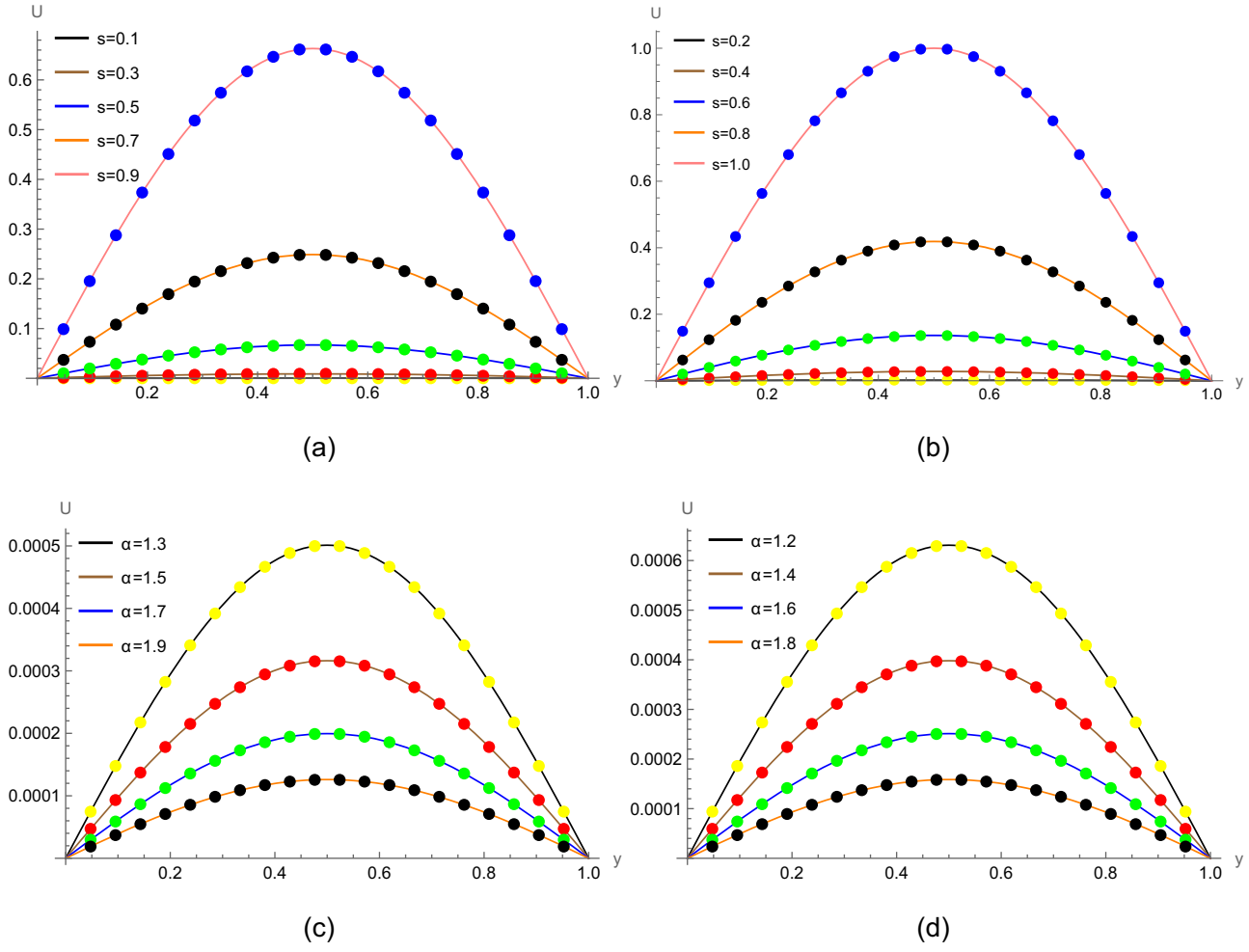

Figure 10: Exact and numerical solutions for Example 7.4 at different time stages. (a) $\mathcal{N} = 100$, $\alpha = 1.9$, $K = 500$; (b) $\mathcal{N} = 100$, $\alpha = 1.9$, $K = 500$; (c) $\mathcal{N} = 100$, $s = 0.1$, $K = 500$; and (d) $\mathcal{N} = 100$, $s = 0.1$, $K = 500$.

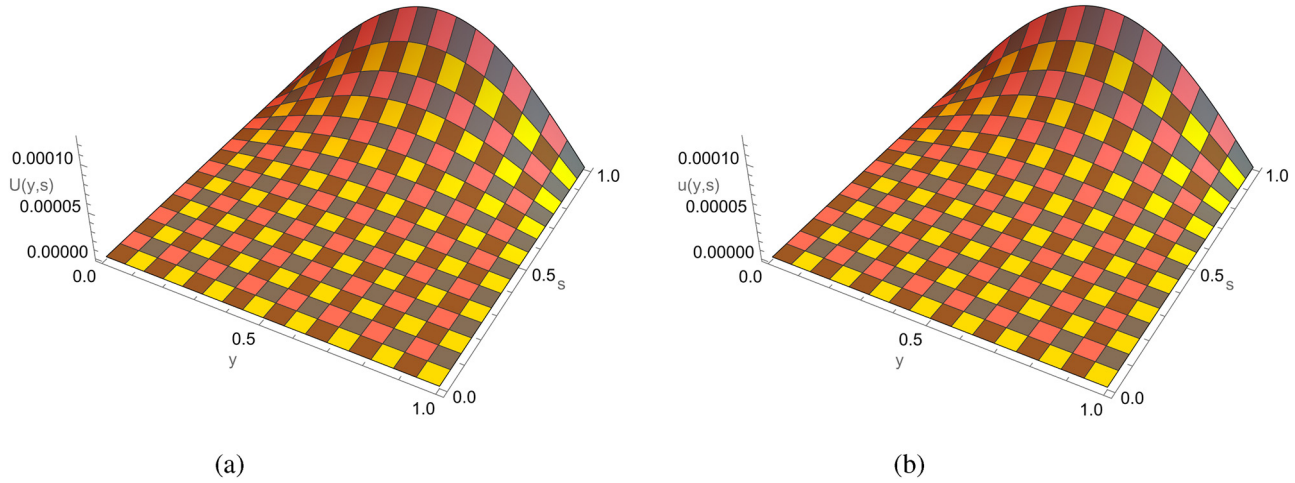

Figure 11: 3D (a) exact and (b) approximate solution for Example 7.4, when $\mathcal{N} = 100$, $\alpha = 1.9$, $\Delta s = 0.0001$, and $s = 0.1$.

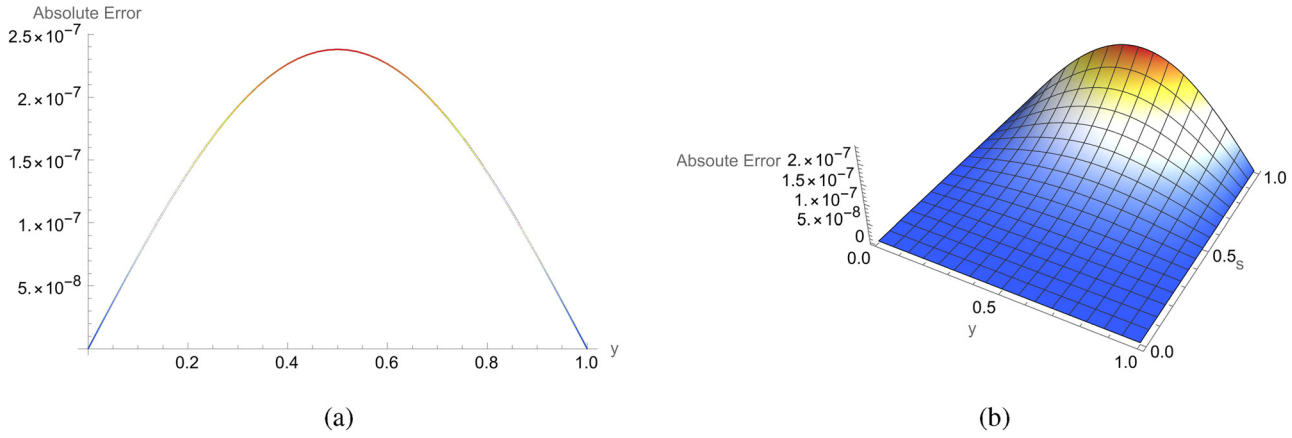

Figure 12: 2D and 3D error profiles of Example 7.4, when $\mathcal{N} = 50$, $\alpha = 1.9$, $\Delta s = 0.0001$, and $s = 0.1$. (a) 2D error function and (b) 3D error function.

is easy to understand, efficient, and practical. This method is reliable as. For many fractional differential equations, this approach can be utilized to obtain effective approximate solutions. It will produce better outcomes for problems that lack an exact solution. The obtained solution to the TFKGE for various time levels has been compared with the exact solution and existing methods by calculating L_∞, L_2 errors. The comparison indicated improved accuracy compared to [30] and [52]. Further research should concentrate on broadening the scope, thoroughly examining the characteristics of the algorithm, and investigating its practical applications.

Acknowledgments: The authors would like to acknowledge the funder from the Ministry of Higher Education, Malaysia; Fundamental Research Grant Scheme (FRGS) Grant code (FRGS/2021/STG06/USM/02/9) and Article Processing Charge (APC) Fund from Research Creativity and Management Office (RCMO), Universiti Sains Malaysia. The authors would like to thank the School of Mathematical Sciences, Universiti Sains Malaysia for research assistance and computing facilities. The authors extend their appreciation to Taif University, Saudi Arabia, for supporting this work through project number (TU-DSPP-2024-47).

Funding information: This research was funded by Taif University, Saudi Arabia, Project No. (TU-DSPP-2024-47).

Author contributions: Muserat Shaheen: methodology, investigation, writing-original draft, writing – review, and editing. Muhammad Abbas: Supervision, project administration, methodology, investigation, writing-original draft, writing – review, and editing. Farah Aini Abdullah: Methodology, investigation, validation, writing-original draft, writing-review and editing. Yasser Salah Hamed: Methodology, investigation, validation, writing-original draft, writing-review and editing. All authors have accepted responsibility for the entire content of this manuscript and approved its submission.

Conflict of interest: The authors state no conflict of interest.

Data availability statement: All data generated or analysed during this study are included in this published article.

References

[1] Atangana A, Baleanu D. New fractional derivative with nonlocal and non-singular kernal: theory and application to heat transfer model. Therm science. 2016;20:763–9.
[2] Caputo M, Febrizio M. A new definition of fractional derivative without singular kernel. Progress Fract Differ Appl. 2015;2:73–85.
[3] Diethelm K, Ford NJ. Multi-order fractional differential equations and their numerical solution. Appl Math Comput. 2004;154:599–894.
[4] El-Sayed AMA, El-Mesiry AEM, El-saka HAA. On the fractional-order logistic equation. Appl Math Lett. 2007;20:817–23.
[5] Shakeri F, Dehghan M. Numerical solution of Klein-Gordon equation via he's variational itrational method. Nonlinear Dynam. 2008;51:89–97.
[6] Onate CA, Ikot AN, Ojonubah JO. Analytical solutions of the Klein-Gordon equation with a combined potential. Chin J Phys. 2016;54:820–9.
[7] Gorka P. Logrithmic Klein-Gordon equation. Acta Phys Polonica B. 2009;40:59–66.
[8] Kunbinarasaiah S. A new approach for the numerical solution for non-linear Klein-Gordon equation. SeMA J. 2020;77:435–56.

[9] Lou SY, Chen WZ. Multidimensional solutions of the nonlinear Klein-Gordon equation. Phys Lett A 1991;156:260–6.
[10] Chatterjee A. Large-N solution of the Klein-Gordon equation. J Math Phys. 1986;27:2331–5.
[11] Subasi M, Araz SI. Numerical regularization of optimal control for the coefficient function in a wave equation. Iran J Sci Tech Trans A Sci. 2019;43:2325–33.
[12] Atangana A, Araz S. II. Extension of Atangana-Seda numerical method to partial differential equations with integer and non-integer order. Alex Eng J. 2020;59:2355–70.
[13] Subasi M, Gungor H, Araz SI. On the control of end point tensions in a vibration problem. Int J Model Optim. 2017;7:74.
[14] Dehghan M, Shokri A. Numerical solution of the nonlinear Klein-Gordon equation using radial basis functions. J Comput Appl Math. 2009;230:400–10.
[15] Berat K., Yusuf U., Murat Y, Alaattin E. A new perspective on the numerical solution for fractional Klein Gordon equation. J Polytechnic. 2019;22:443–51.
[16] Bratsos AG. On the numerical solution of the Klein-Gordon equation. Numer Methods Partial Differ Equ. 2009;25:939–51.
[17] Zhang Z, Fuzhang WANG, Zhang J. The space-time meshless methods for the solution of one-dimensional Klein-Gordon equations. Wuhan Univ J Nat Sci. 2022;27:313–20.
[18] Shakeri F, Dehghan M. Numerical solution of the Klein-Gordon equation via He's variational iteration method. Nonlinear Dyn. 2007;51:89–97.
[19] Ganji RM, Jafari H, Kgarose M, Mohammadi A. Numerical solutions of time-fractional Klein-Gordon equations by clique polynomials. Alex Eng J. 2021;60:4563–71.
[20] Saifullah S, Ali A, Khan ZA. Analysis of nonlinear time-fractional Klein-Gordon equation with power. AIMS Math. 2022;7:5275–90.
[21] Liu J, Nadeem M, Habib M, Akgul A. Approximate solution of nonlinear time-fractional Klein-Gordon equations using Yang transform. Symmetry. 2022;14:907.
[22] Bentrcia T, Mennouni A. On the solution behavior of a nonlinear time-fractional Klein-Gordon equation: Theoretical study and numerical validation. Commun Nonlinear Sci Numer Simulat. 2023;125:1007–5704.
[23] Chen H, Lu S, Chen W. A fully discrete spectral method for the nonlinear time fractional Klein-Gordon equation. Taiwan J Math. 2017;21:231–51.
[24] Mohebbi A, Abbaszadeh M, Dehghan M. High-order difference scheme for the solution of linear time fractional Klein-Gordon equations. Numer Methods Partial Differ Equ. 2014;30:1234–53.
[25] Hassani H, Machado JAT, Naraghirad E. An efficient numerical technique for variable order time fractional nonlinear Klein-Gordon equation. Appl Numer Math. 2020;154:260–72.
[26] Vivas-Cortez M, Huntul MJ, Khalid M, Shafiq M, Abbas M, Iqbal MK. Application of an Extended Cubic B-spline to find the numerical solution of the generalized nonlinear time-fractional Klein-Gordon equation in mathematical physics. Computation. 2024;12:80.
[27] Ahmad Z, Crisci S, Murtaza S, Toraldo G. Numerical insights of fractal-fractional modeling of magnetohydrodynamic Casson hybrid nanofluid with heat transfer enhancement. Math Methods Appl Sci. 2024;47:9046–66.
[28] Ahmad Z, Bonanomi G, Cardone A, Iuorio A, Toraldo G, Giannino F. Fractal-fractional sirs model for the disease dynamics in both prey and predator with singular and nonsingular kernels. J Biol Syst. 2024;25:1–34.
[29] Ahmad Z, Bonanomi G, di Serafino D, Giannino F. Transmission dynamics and sensitivity analysis of pine wilt disease with asymptomatic carriers via fractal-fractional differential operator of Mittag-Leffler kernel. Appl Numer Math. 2023;185:446–65.
[30] Amin M, Abbas M, Iqbal MK, Baleanu D. Numerical treatment of time-fractional Klein-Gordon equation using redefined Extended Cubic B-Spline functions. Front Phys. 2020;288:1–13.
[31] Sarboland M, Aminataei A. Numerical solution of the nonlinear Klein-Gordon equation using multiquadric quasi-interpolation scheme. Univ J Appl Math. 2015;3:40–9.
[32] Amin R, Shah K, Mlaiki N, Yaaazbasi S, Abdeljawad T, Hussain A. Existence and numerical analysis using Haar wavelet for fourth-order multi-term fractional differential equations. Comput Appl Math. 2022;41:329.
[33] Amin R, Yuzbasi S, Nazir S. Efficient numerical scheme for the solution of HIV infection CD4+ T-cells using Haar wavelet technique. CMES-Comput Model Eng Sci. 2022;131:639–53.
[34] Saeed U., ur Rehman M. Hermite wavelet method for fractional delay differential equations. J Differ Equ. 2014;2014:359093.
[35] Mohammadi F, Cattani C. A generalized fractional-order Legendre wavelet Tau method for solving fractional differential equations. J Comput Appl Math. 2018;339:306–16.
[36] Amin R, Yuzbasi S, Gao L, Asif M, Khan I. Algorithm for the numerical solutions of volterra population growth model with fractional order via Haar wavelet: Haar wavelet method for volterra population growth model with fractional order. Contemporary Math. 2020;102–11.
[37] Yousif MA, Hamasalh FK. Novel simulation of the time fractional Burgers-Fisher equations using a non-polynomial spline fractional continuity method. AIP Adv. 2022;12:115018.
[38] Algehyne EA, Ibrahim M. Fractal-fractional order mathematical vaccine model of COVID-19 under non-singular kernel. Chaos Solitons Fractals. 2021;150:111150.
[39] Al-Raeei M. Applying fractional quantum mechanics to systems with electrical screening effects. Chaos Solitons Fractals. 2021;150:111209.
[40] Mittag-Leffler GM. Sur la nouvelle function $E_\alpha(X)$. C R Acad Sci Paris. 1903;137:554–8.
[41] Shukla AK, Prajapati JC. On a generaization of Mittag-Leffler function and its properties. J Math Anal Appl. 2007;336:797–811.
[42] Poulin JR. Calculating infinite series using Parsevals identity (master thesis), Orono: The University of Maine; 2020.
[43] De Boor C. On the convergence of odd-degree spline interpolation. J Approx Theory. 2009;1:452–63.
[44] Shafiq M, Abbas M, Abdullah FA, Majeed A, Abdejawad T, Alqudah MA. Numerical solution of time fractional Burgers' equation involving Atangana-Baleanu derivative via cubic B-spline function. Results Phys. 2022;34:105244.

[45] Siddiqi SS, Arshed S. Quintic B-spline for the numerical solution of the good Boussinesq equation. J Egypt Math Soc. 2014;22(2):209–13.
[46] Khalid N, Abbas M, Iqbal MK. A numerical investigation of caputo time fractional allen-cahn equation using redefined cubic b-spline functions. Adv Differ Equ. 2020;158:1–22.
[47] Akram T, Abbas M, Ali A. A numerical study on time fractional fisher equation using an extended cubic b-spline approximation. J Math Comput Sci. 2021;22:85–96.
[48] Kadalbajoo MK, Arora P. B-spline collocation method for the singular-perturbation problem using artificial viscosity. Comput Math Appl. 2009;57:650–63.
[49] Hal C. On error bounds for spline interpolation. J Approx Theory. 1968;1:209–18.
[50] Yadav S, Pandey RK, Shukla AK. Numerical approximation of Atangana-baleanu caputo derivative and its application. Chaos Solitons Fract. 2019;118:58–64.
[51] Odibat Z, Momani S. The variational iteration method: an efficient scheme for handling fractional partial differential equations in fluid mechanics. Comput Math Appl. 2009;58:2199–208.
[52] Nagy A. Numerical solution of time fractional nonlinear Klein-Gordon equation using Sinc-Chebyshev collocation method. Appl Math Comput. 2017;310:139–48.